



**HAL**  
open science

# The directionality of collective cell delamination is governed by tissue architecture and cell adhesion in a *Drosophila* carcinoma model

Marta Mira-Osuna, Steffen Plunder, Eric Theveneau, Roland Le Borgne

## ► To cite this version:

Marta Mira-Osuna, Steffen Plunder, Eric Theveneau, Roland Le Borgne. The directionality of collective cell delamination is governed by tissue architecture and cell adhesion in a *Drosophila* carcinoma model. 2024. hal-04779250

**HAL Id: hal-04779250**

**<https://hal.science/hal-04779250v1>**

Preprint submitted on 13 Nov 2024

**HAL** is a multi-disciplinary open access archive for the deposit and dissemination of scientific research documents, whether they are published or not. The documents may come from teaching and research institutions in France or abroad, or from public or private research centers.

L'archive ouverte pluridisciplinaire **HAL**, est destinée au dépôt et à la diffusion de documents scientifiques de niveau recherche, publiés ou non, émanant des établissements d'enseignement et de recherche français ou étrangers, des laboratoires publics ou privés.

## **The directionality of collective cell delamination is governed by tissue architecture and cell adhesion in a *Drosophila* carcinoma model**

**Running title:** Septate junction integrity loss and *Ras*<sup>V12</sup> elicit collective delamination

Marta Mira-Osuna<sup>1</sup>, Steffen Plunder<sup>2,3</sup>, Eric Theveneau<sup>2</sup>, Roland Le Borgne<sup>1</sup>

### **Affiliations**

Marta Mira-Osuna, ORCID : 0009-0007-0243-1540

<sup>1</sup>Institut de Génétique et Développement de Rennes (IGDR), Université de Rennes, CNRS UMR 6290, F-35000 Rennes, France.

Steffen Plunder, ORCID: 0000-0002-3371-3790

<sup>3</sup> Institute for the Advanced Study of Human Biology (ASHBi), Kyoto University Institute for Advanced Study, Kyoto University, Yoshida-Konoe-cho, Sakyo-ku, Kyoto 606-8501, Japan.

Eric Theveneau, ORCID: 0000-0001-6510-5717

<sup>2</sup> Molecular, Cellular and Developmental biology department (MCD), Centre de Biologie Integrative (CBI), University of Toulouse, CNRS, UPS, 31062 Toulouse, France.

Roland Le Borgne, ORCID : 0000-0001-6892-278X

<sup>1</sup>Institut de Génétique et Développement de Rennes (IGDR), Université de Rennes, CNRS UMR 6290, F-35000 Rennes, France.

**Key words:** epithelia, septate junctions, *Ras*<sup>V12</sup>, extrusion, delamination, carcinoma

## Abstract

Carcinomas originate in epithelia and are the most frequent type of cancers. Tumor progression starts with the collective delamination of live tumors out of the epithelium, and requires modulation of cell adhesion. Yet, it remains elusive exactly how remodeling of epithelial cell-cell and cell-extracellular matrix contacts contribute to metastasis onset and delamination directionality. We used *Drosophila melanogaster* larval eye disc to study cooperative oncogenesis and determine the contribution of bi- and tricellular septate junction (SJ) components to tumor progression in flat and pseudostratified epithelia. We reveal that loss-of-function of septate junction components alone can promote cell death whereas synergic interaction with oncogenic Ras triggers the collective delamination of living tumorigenic cells. Spatiotemporal analyses reveal apical and basal delamination processes differ in terms of cell identity, cell polarity and remodeling of cell-cell and cell-ECM contacts. Using a combination of *in vivo* and *in silico* approaches, we report that SJ-depleted  $Ras^{V12}$  tumors in pseudostratified epithelia trigger tissue folding or basal collective delamination regardless of the order in which cell contacts are remodeled. In striking contrast, SJ-depleted  $Ras^{V12}$  tumors formed in flat, squamous epithelia, first undergo apical constriction and acquire a dome-like shape. Tumors are enriched in adhesion molecules and form an apical neck at the interface of contact between mutant cells and wild-type neighbors. Concomitant to cytoskeleton remodeling, tumors emit apical protrusions in the lumen and progressively delaminate through the apical neck while remaining cohesive. Our study reveals that tissue architecture and changes in cell adhesion drive the directionality of collective delamination of neoplastic tumors out of an epithelium.

## Introduction

Epithelial tissues compartmentalize the organism into organs, multicellular rearrangements carrying out highly specialized functions. Epithelia are composed of one or multiple layers of polarized epithelial cells in which apico-basolateral polarity modules are spatially restricted, creating plasma membrane domains to which junctional complexes are localized (Buckley & St Johnston, 2022; Campanale et al., 2017; Flores-Benitez & Knust, 2016; Pickett et al., 2019; Tepass, 2012; Vasquez et al., 2021). At the interface of contact between two or three adjacent cells, bicellular and tricellular junctions form, respectively. In invertebrates like *Drosophila*, adherens junctions are formed by E-cadherin (E-cad)-Catenins complexes and are localized at the apical domain. Adherens junctions mediate intercellular adhesion and are linked to the actomyosin cytoskeleton, mechanically coupling neighboring cells together and establishing the mechanical barrier of the tissue. Septate junctions (SJ), considered somewhat analogous to the vertebrate tight junctions, are located at the basolateral domain and comprise over 30 biochemically diverse proteins, of which core-complex components include Coracle (Cora) and Nervana 2 (Nrv2). SJ regulate selective permeability across the epithelium upon establishment of a mature paracellular diffusion barrier, which becomes functional in late-embryogenesis (Baum & Georgiou, 2011; Guillot & Lecuit, 2013; Harris & Tepass, 2010; Izumi & Furuse, 2014; Oshima & Fehon, 2011). Loss-of-function of bicellular SJ core-components *nrv2* and *cora* in early embryonic stages results in embryonic lethality, suggesting bicellular SJ may contribute to epithelia homeostasis beyond their barrier functions (Genova & Fehon, 2003; Hall & Ward, 2016; Paul et al., 2003). In recent years, tricellular junctions have emerged as essential regulators of epithelia homeostasis across metazoans. Tricellular junctions function as hubs for mechanochemical signaling throughout development, acting as spatial landmarks for spindle orientation during cell division, sites for epithelia integration in cell migration and regulating cell intercalation during tissue convergent-extension (Finegan et al., 2019; Higashi et al., 2016; Ikawa et al., 2023; Ventura et al., 2022; Wang et al., 2018). Tricellular SJ form at the level of SJ and by three vertex-restricted proteins: the proteolipid protein M6, the triple-repeat protein Anakonda (Aka), and the transmembrane protein Gliotactin (Gli). Loss-of-function of *M6* or *aka*, upstream regulators of tricellular SJ assembly, results in early embryo lethality (Byri et al., 2015; Zappia et al., 2011), at stages 13, when the permeability barrier is not yet mature and the embryo undergoes intensive morphogenesis.

At the interface of contact between cells and the extracellular matrix (ECM), focal adhesions mediate mechanotransduction and signaling between cells and the extracellular matrix via heterodimeric integrin receptors coupled to the basal actin cytoskeleton. The ability of cells to coordinate their behavior in response to intrinsic genetic programs and extrinsic stimuli drives tissue-scale organizations and preserves homeostasis. Across development, the orchestration of novel multicellular rearrangements during cell division, intercalation and extrusion, requires a tightly controlled cross-talk between polarity cues, changes in adhesiveness and actomyosin-based contractility and force generation (Mira-Osuna & Le Borgne, 2024). In turn, mechanochemical cues converge at the cell interface where cell junctions must be robust, to sustain mechanical tension and prevent tissue rupture. At the same time and paradoxically, cell junctions must remain plastic, to modulate cell adhesion and packing. Junctional remodeling comprises the reinforcement, *de novo* assembly and disassembly of junctional complexes to enable tissue integrity maintenance in developing and mature epithelia.

Proteins of the rat sarcoma viral oncogene family (Ras) are involved in key cellular processes during development, from proliferation to differentiation, and appear mutated in ~19% of patients with cancer worldwide, in human cancers with some of the highest mortality rate (Prior et al., 2020). The human oncogenes *K-Ras*, *H-Ras* and *N-Ras* have only one homologue in *Drosophila*, the oncogene Ras1 (Ras<sup>85D</sup>) (Simon et al., 1991). Ectopic expression of overactivated Ras1 (Ras<sup>G12V</sup> also called Ras<sup>V12</sup>) causes developmental defects and promotes tumorigenic growth (Duchek & Rorth, 2001; Karim & Rubin, 1998; Yang & Baker, 2003). Metastasis starts with the deviation of tumors from the cell layer in a process known as epithelial-to-mesenchymal transition (EMT) (Yang et al., 2020). This first step in tumor progression is critical and the directionality in which cells leave an epithelium has a major impact on cell fate, tumor invasiveness, and ultimately, survival. Tissue-clearance processes, namely cell competition, prevent tumor initiation by inducing caspase-activation and extrusion of potentially hazardous cells (Cong & Cagan, 2024). Cell extrusion occurs apically in vertebrates and basally in invertebrates, and extruded cell ultimately die (Marinari et al., 2012; Monier et al., 2015; Rosenblatt et al., 2001; Teng et al., 2017; Villars et al., 2022). However, oncogenic mutations like Ras<sup>V12</sup> block cell death and can synergize with other genetic insults to revert the directionality of epithelial deviation and promote tumor progression (Dillard et al., 2021; Wu et al., 2010). As a result, tumors undergo delamination, deviating collectively and alive out of the epithelium, heightening tumor malignancy (Gudipaty & Rosenblatt, 2017; Ohsawa et al., 2018). The molecular regulators governing the directionality of this three-dimensional rearrangement start to be elucidated (Slattum et al., 2009; Tamori et al., 2016; Villars et al., 2022). However, how this machinery is orchestrated together with junctional rearrangements, such as the dismantling of junctional complexes, remains poorly understood. Constitutive activation of MyoII in Ras<sup>V12</sup> tumors promotes basal deviation from the epithelium (Dunn et al., 2018). Null mutation of the tricellular septate junction component M6 synergizes with Ras<sup>V12</sup> and activates Rho-1 signaling. Subsequent remodeling of the cytoskeleton network is coupled to adherens junctions remodeling via Canoe (Manning et al., 2019; Sawyer et al., 2009; Yu & Zallen, 2020) and promotes tumor deviation both apically and basally (Dunn et al., 2018). Whether this is exclusive to M6, or can be a broader function of SJ in preserving the epithelial barrier remains unclear. The body of evidence highlighting bicellular SJ involvement in embryonic morphogenesis, M6 in carcinogenesis and the recently described interplay between bicellular and tricellular SJ, suggest SJ may contribute to epithelia homeostasis beyond paracellular diffusion barrier functions. However, how SJ integrity contributes to epithelial homeostasis in the context of tumor progression remains unknown.

To explore the potential role SJ play in tumor progression, we make use of the larval eye-antenna imaginal disc of *Drosophila melanogaster*, a model in cancer biology used to characterize oncogenic Ras interaction with additional mutations in which hallmarks of human cancers are recapitulated (Dillard et al., 2021; Miles et al., 2011; Pagliarini & Xu, 2003; Vidal & Cagan, 2006). The immature visual organ of *Drosophila* is composed of two cell layers: an outer flat epithelium (peripodial epithelium, PE) and an inner pseudostratified epithelium (disc proper, DP), separated by a lumen and facing each other through their apical domains. During larval development, the pseudostratified epithelium undergoes neurogenesis and terminal differentiation is mediated by cell-cell interactions, independently of cell lineage. The forefront of the posterior-to-anterior wave of differentiation is called the morphogenetic furrow (MF) and can be observed as a transient indentation in the

pseudostratified epithelium (Wolff & Ready, 1991). From larval stage L3 stage (L3 stage) until 24h after puparium formation, the initial pool of equipotent progenitors is sequentially specified in neuronal photoreceptors or accessory cells and patterned into an ommatidia lattice (Cagan & Ready, 1989; Wolff & Ready, 1991). Eye development culminates with the formation of a neuro-crystalline ommatidia lattice, a functional visual organ. In this study, we reveal how loss of SJ integrity in synergy with oncogenic Ras triggers apical and basal collective delamination of living cells in the *Drosophila* larval eye, the onset of metastasis and first step in tumor progression. Using spatiotemporal analyses of fixed specimen and mathematical modeling, we find that directionality of collective delamination is governed by tissue architecture and changes in cell adhesion. By developing a minimal theoretical model of collective delamination, we show that flat epithelia are highly sensitive to order in which junctional complexes are remodeled, while pseudostratified epithelia are not, and in both cases mutant cells require preferential adhesion to deviate collectively. We find, both *in silico* and *in vivo* that mutant cells in the flat epithelium exclusively undergo apical collective delamination. Conversely, mutant cells in the pseudostratified epithelium undergo collective cell movements, forming tissue folding and rosettes, the latter resulting from basal collective delamination. Our results unveil a novel role for SJ in preventing tumor progression and provide an understanding on how collective delamination is governed by tissue intrinsic features and cell adhesion to deviate living cells out of an epithelium, the first event in tumor progression.

## Results

### **Loss of septate junction integrity in larval eye-antennal disc epithelium induces caspase activation and cell extrusion**

First, we studied whether loss of SJ integrity in postembryonic epithelia is detrimental for cell survival. We used the larval eye-antennal imaginal disc and generated genetically heterozygote tissues containing wild-type cells and clones of mutant cells homozygote for recessive lethal SJ alleles. The eye disc is a developing organ that undergoes neurogenesis from L3 until 24h after pupariation (Ready et al., 1976). The morphogenetic furrow (MF) is the forefront of differentiation and can be identified as the transient apical constriction and indentation of the pseudostratified epithelium (Fig. 1A, B). The MF progresses across the eye field in a posterior-to-anterior fashion. Cells anterior to the MF are equipotent and become progressively patterned into an ommatidia lattice, posterior to the MF (Wolff & Ready, 1991). In cells from the flat and in the pseudostratified epithelium, adherens junctions main component E-cadherin (E-cad) is located apical to the bicellular SJ core-complex component Cora (Fig. 1A) and tricellular SJ components Aka and Gliotactin (Gli) (Fig. S1A), as described in the pupal notum (Esmangart de Bourmonville & Le Borgne, 2020). Since loss of core SJ components is embryonic lethal, we used the Mosaic Analysis with Repressible Clone Marker (MARCM) system to generate genetic mosaicism in the developing organ. The tissue-restricted ey-Flipase (ey-Flp) was expressed under control of the *eyeless* promoter. In combination with the UAS/Gal4/Gal80 system, mitotic FRT-site specific recombination was induced and clones tagged with the GFP clone marker were generated (Germani et al., 2018; Luo & Wu, 2007). Previous studies reported synergic interaction with *Ras*<sup>V12</sup> resulted in cells deviating from the epithelium (Dunn et al., 2018). Hence, we first sought to confirm

whether loss-of-function of the M6 null allele ( $M6^{W186Stop}$ ) resulted in cells undergoing caspase-activated cell extrusion or live cell delamination.

Cell extrusion is the process by which junctional complexes are sequentially remodeled to seamlessly remove caspase-activated cells from the epithelium (Levayer, 2024). We observed homozygote M6 mutant cells, from here forth referred to as “clones mutant for M6” expressed the GFP-clone marker (Fig. 1D, F, green arrowheads). Clones mutant for M6 were generated in the flat (Fig. 1D) and pseudostratified epithelium, anterior (Fig. 1F) and posterior (Fig. S1B) to the MF. Clones mutant for M6 contained pyknotic nuclei (Fig. 1D, F, S1B, orange arrowheads), highly condensed spheres of DAPI-marked DNA, a sign of apoptotic activation. Caspase-activated cell extrusion is a cell competition mechanism used to eliminate polarity deficient cells from a genetically mosaic tissue when not in synergy with oncogenic Ras (Amoyel & Bach, 2014; Brumby & Richardson, 2003; Dillard et al., 2021; Igaki et al., 2009; Menéndez et al., 2010). We next studied whether clones mutant for M6 with pyknotic nuclei underwent apoptosis and cell extrusion. In the eye disc, developmentally programmed cell-death occurs during pupation in the pseudostratified epithelium, posterior to the MF, to remove the excess of unpatterned cells (Wolff & Ready, 1991). We therefore quantified cell death in the eye disc at larval stages, before developmentally programmed cell-death starts. To this aim, we made use of the marker of early caspase activation cleaved-*Drosophila* caspase-1 (cDcp1) (Fig. 1D, F, violet arrowheads). We observed over half of M6 mutant cells in the flat epithelium (Fig. 1D) and anterior to the MF in the pseudostratified epithelium (Fig. 1F) were positive for cDcp1 during L2 and early L3 larval stages. Therefore, M6 loss in flat and pseudostratified epithelia promotes caspase-activation and cell extrusion of M6-deficient cells. We next studied whether caspase-activated extrusion in M6 clones was a specific role of M6 independent of SJ, or whether it results from the disruption of SJ integrity. We studied loss-of-function mutations of bi- and tri-cellular SJ components. Single loss-of-function mutation of tricellular SJ master regulator *Aka* ( $aka^{L200}$ , null allele (Byri et al., 2015)) or bicellular SJ core-component *Nrv2* ( $nrv2^{K13315}$ , hypomorphic allele (Genova & Fehon, 2003)) recapitulated the above described observations for M6. Clones of *aka* or *nrv2* mutant cells were located in the flat (Fig. S1C, E) and pseudostratified epithelium (Fig. S1D, F) of the eye disc and were identified by the nucleus-restricted nls GFP clone marker. In these clones, nuclei were fragmented into spherical bodies, very reminiscent to pyknotic nuclei (Fig. S1C-F, orange arrowheads). Thus, mutant clones for *aka* and *nrv2* strongly resembled caspase-activated M6 clones undergoing cell extrusion. These results show loss of bi- or tri-cellular SJ components, hence SJ integrity, does not trigger detectable tissue deformation in the larval eye disc. However, SJ integrity prevents cell elimination and SJ deficient cells undergo caspase-activation and cell extrusion, possibly due to cell competition mechanisms triggered in wild-type neighbors.

### **Loss of septate junction integrity synergizes with Ras overactivation to induce collective delamination**

M6 loss has been observed to synergize with  $Ras^{V12}$  and induce tumor invasion in *Drosophila* (Dunn et al., 2018). Hence, we next studied the role of bicellular and tricellular SJ components in the context of tumorigenesis to determine whether SJ integrity functions to prevent tumor progression. We induced mutant clones of a tricellular ( $M6^{W186Stop}$ ,  $aka^{L200}$ ,  $gfp^{DV3}$ ) or bicellular ( $nrv2^{K13315}$ ) SJ component, in synergy with  $Ras^{V12}$ , to make cells refractory to apoptosis. Clones with oncogenic Ras and M6 null allele underwent apical and basal collective delamination, appearing deviated in the lumen or basal to the eye disc,

respectively (Fig1G-I). Moreover, we observed no sign of caspase activation in neither clones deviated apically (Fig. S2A, B) nor basally (Fig. S2C). This suggests M6-deficient tumors delaminate collectively and alive out of the epithelium. We also generated clones of cells homozygote mutant for other tricellular (*aka*<sup>L200</sup>, *glt*<sup>PV3</sup>) or bicellular (*nrv2*<sup>K13315</sup>) SJ components in synergy with *Ras*<sup>V12</sup>. Tricellular SJ-deficient tumors underwent apical (Fig. S2E) and basal collective delamination (Fig. S2F). Similarly, loss of bicellular SJ in tumors also promoted the apical (Fig. S2G) and basal (Fig. S2H) collective delamination of living cells out of the epithelium. Together, these observations show loss of SJ integrity in tumors triggers the collective delamination of cells alive out of the epithelium, both apically and basally. Multicellular organization and localization of E-cad differed between apically and basally delaminated clones. SJ-deficient *Ras*<sup>V12</sup> cells that underwent apical collective delamination clustered in the lumen and E-cad localized along cell membranes (Fig. 1H, S2B, E, G). Conversely, SJ-deficient *Ras*<sup>V12</sup> cells that underwent basal collective delamination formed basal rosettes, radial structures in which E-cad was restricted to the central domain (Fig1E-F). Hence, we next characterized the remodeling of junctional complexes and the actomyosin network to decipher how together they orchestrate apical and basal collective delamination.

### **Tissue folding in the pseudostratified epithelium exhibits different junctional remodeling in clones anterior and posterior to the MF**

We next set to decipher the sequence of events leading up to apical and basal collective delamination. We staged larval eye-antenna imaginal discs at different time-windows during larval development and performed spatiotemporal analyses of fixed specimen (see Methods). We stained for cell-cell and cell- extracellular matrix adhesion proteins, E-cad and  $\beta$ -integrin, respectively. We also characterized cytoskeleton remodeling using the phosphorylated regulatory light chain of non-muscle type II myosin (P-Myo) as a proxy for active MyoII and filamentous actin (F-actin). First, we studied SJ-deficient tumors located in the undifferentiated region of the pseudostratified epithelium, anterior to the MF. From late L2 until L3 stages, a gradation in the phenotype of clones was associated with clone size. Small clones were wild-type-like and did not showcase any difference in terms of junctional markers or cytoskeleton remodeling in comparison to adjacent wild-type neighbors. (Fig. 2A-C). Intermediate size clones exhibited apical constriction and basolateral spreading of E-cad and P-Myo, and remained basally anchored to the extracellular matrix via  $\beta$ -integrin (Fig. 2D-F). Large clones formed tissue folds and showcased apical constriction as well as basolateral spreading of E-cad and P-Myo. Strikingly,  $\beta$ -integrin in large clones was no longer restricted to the basal pole and instead appeared globally increased at the lateral and apical cortex (Fig. 2G-I). We next focused on SJ-deficient tumors located posterior to the MF, in the differentiated region of the pseudostratified epithelium. These clones also had a gradation in phenotype but showcased different junctional remodeling to anteriorly located clones. During L3 stages, small clones posterior to the MF underwent apical constriction concomitant with loss of E-cad basally and detachment from the extracellular matrix, evidenced by the basal loss of  $\beta$ -integrin and actin stress fibers (Fig. 3A-C). Bigger clones formed deeply invaginated epithelial folds and also showcased apical constriction concomitant to the basal loss of E-cad,  $\beta$ -integrin and F-actin. Strikingly, tissue folds were additionally enriched in  $\beta$ -integrin at the apical cortex (Fig. 3F). Altogether, these results indicate that synergic interaction between the loss of SJ integrity and *Ras*<sup>V12</sup> in the pseudostratified epithelium severely disrupts tissue architecture, triggering collective cell movements with a basal directionality.



Junctional and cytoskeleton remodeling during epithelia folding is strikingly different in SJ-deficient tumors located anterior and posterior to the forefront of neural differentiation. Furthermore, differences in adhesiveness between mutant cells and their wild-type counterparts may be essential for tissue fold formation in this tissue.

### **Rosettes are composed of differentiated cells delaminating from SJ-deficient *Ras*<sup>V12</sup> tumors in the pseudostratified epithelium**

We next studied cell identity and polarity markers in addition to junctional components to decipher the origin of rosettes formed upon basal delamination of SJ-deficient tumors. Rosettes systematically appeared as a cluster of mutant cells organized radially, detached from the cell layer and located basal to the eye disc. We stained for Elav, a marker of early neural differentiation (Robinow & White, 1991), and the atypical protein kinase C (aPKC), a component of the apical Par polarity complex (Wodarz et al., 2000). Anterior to the MF, intermediate-size clones undergoing apical constriction were formed by a homogenous population of undifferentiated Elav-negative mutant cells (Fig. 4A, B). Moreover, basolateral E-cad delocalization at this stage was accompanied by a partial delocalization of aPKC to the basal pole, suggesting a partial loss of polarity (Fig. S3A-B). Similarly, large clones in this region forming tissue folds comprised a homogenous population of undifferentiated, Elav-negative mutant cells (Fig. 4C, D). In these clones, E-cad basolateral delocalization and aPKC partial basal delocalization suggested an overall alteration of the apico-basal polarity (Fig. S3C, D). Conversely, posterior to the MF, small clones undergoing apical constriction and basally depleted in E-cad were composed of a homogenous Elav-positive mutant cell population (Fig. 4E, F). In these clones, aPKC was apically restricted, suggesting polarity is unaltered (Fig. S3E, F). Similarly, large clones forming tissue folds in this region also comprised a homogeneously Elav-positive cell population (Fig. 4G, H). In these clones, polarity was preserved and aPKC appeared to be restricted apically like in wild-type neighbors (Fig. S3G, H). Basal delaminated rosettes systematically appeared basal to the differentiated region of the pseudostratified epithelium formed by Elav-positive, polarized cells (Fig. 4I, J). In rosettes, aPKC was restricted to the apical domain, where adhesion components E-cad and  $\beta$ -integrin were also localized (Fig. S3I-K). Based on their location, the expression of Elav and their polarity status, we propose rosettes originate from SJ-deficient tumor located in the pseudostratified epithelium, posterior to the MF, that undergo basal collective delamination.

### **SJ-deficient *Ras*<sup>V12</sup> tumors delaminate apically from the flat epithelium**

Our spatiotemporal analyses on fixed specimen revealed that SJ-deficient tumor generated in the flat epithelium systematically underwent apical collective delamination in the lumen. First, at the beginning of L3, in the early stages of apical collective delamination, *M6*<sup>VW186Stop</sup>*Ras*<sup>V12</sup> clones had an average size of 6 cells ( $\pm 2$ ), underwent apical constriction and acquired a dome-like shape on the basal side. On the apical side, clones formed a neck in the plane of adherens junctions and emitted cytoplasmic apical protrusions into the lumen. Because of their morphology, we have named them octopus-shaped clones. This stage is characterized by the lateral enrichment of E-cadherin and  $\beta$ -integrin between *M6*<sup>VW186Stop</sup>*Ras*<sup>V12</sup> cells (Fig. 5A-C). Next, until 115hAEL, clone sized increased to 13 cells ( $\pm 5$ ) and mutant cells were observed to translocate into the lumen through the apical neck (blue arrow, Fig. 5E). Mutant cells remained all connected, indicative of a collective delamination, and  $\beta$ -integrin appeared enriched in the entire clone (Fig. 5D-F). More

precisely,  $\beta$ -integrin was enriched at the cell membrane of mutant cells in the flat epithelium, in those delaminating through the apical neck and in those successfully deviated in the lumen. From 114hAEL until 120hAEL, in the last step of apical collective delamination, cluster size was 18 cells ( $\pm 5$ ) and mutant cells were totally detached from the cell layer (Fig. 5G, H). Mutant cells appeared collectively delaminated in the lumen and enriched in adhesion proteins like  $\beta$ -integrin (Fig. 5I). Altogether, these *in vivo* results show SJ-deficient tumors exclusively undergo basal collective delamination when originated in the pseudostratified epithelium and apical collective delamination when formed in the flat epithelium. This suggest that cell morphology and the sequential remodeling of cell junctions are key to ensuring the cohesion and directionality of collective delamination of SJ-deficient tumors alive out of an epithelium.

### **Computational modeling recapitulates how flat and pseudostratified epithelia respond differently to epithelial destabilization events**

To further assess the putative importance of the tissue organization and of the various events taking place prior to cell delamination, we turned to computational modelling. We adjusted a recently developed 2D agent-based model of epithelial dynamics (Despin-Guitard et al., 2024; Plunder et al., 2024) (Fig. 6A, see Methods, Supplementary Table 1) to obtain a flat monolayer (Fig. 6B, movieS1) or a short pseudostratified organization (Fig. 6C, movieS1) as observed in the eye-antennal imaginal discs. We implemented for the clone cells apical constriction (event **ApC**), loss of apical cell-cell adhesion (event **A**) and loss of basal adhesion to the cell-matrix (event **B**) and monitored the rate of apical and basal delamination (Fig. 6D). We started by simulating these events either independently or occurring sequentially in various orders, in a single cell, in both types of epithelia (Fig. 6E). All events are progressively implemented over 20 hours of simulation and the epithelia are left to further develop for an extra 30h after the last event took place. **ApC** alone does not trigger delamination on either side but leads to a basal displacement of cell nuclei in the pseudostratified tissue (Fig S4). Interestingly, overall epithelial destabilization in the flat epithelium preferentially leads to apical delamination (Fig. 6E), unless **B** is the first event (Fig. 6E) in which case delamination is randomized. By contrast, in the short pseudostratified tissue basal delamination is systematically the main outcome regardless of the scenario (Fig. 6E-F).

### **Clone size and lateral adhesion contribute to decision making in collective cell delamination**

Next, we asked whether the outcome of epithelial destabilization was sensitive to clone size. In 3D, clone size is tripled to the corresponding size in the 2D-agent model. Hence, we utilized our *in vivo* data to restrain the size of cell populations undergoing delamination *in silico* to study biologically relevant scenarios. We first focused on the **ApC A B** scenario, which involves all events likely to happen *in vivo* based on the above characterized spatiotemporal analyses and leads to the expected directionality of delamination in each tissue, respectively apical and basal for the flat and pseudostratified epithelia. Increasing the clone size in the flat epithelium progressively increases the rate of basal delamination up to 25% of the cells (Fig. 6G, movieS2). By contrast, the impact of increasing the clone size in the pseudostratified epithelium was marginal (Fig. 6G, movieS2). One striking observation from these simulations is that there is a splitting of the clones, i.e. not all cells from the clone extrude on the same side of the epithelium (MovieS2). This was not observed *in vivo*. This

strongly suggests that *in vivo* collective cell delamination requires cell-cell adhesion between mutant cells to be maintained.

### **Lateral adhesion between delaminating mutant cells and their wild-type neighbors ensures directionality**

To assess the impact of cell-cell adhesion, we introduced a new event called **Ai** (for event **A** only at the interface between control cells and clone cells). During this event, clone cells lose apical cell-cell adhesions only at the interface between them and the control cells of the tissue. Normal apical cell-cell adhesions between clone cells are maintained. When **Ai** occurs, the two control cells on either side of the clone form a new bond and “heal” the local wound (see Methods). In the pseudostratified tissue, maintaining adhesion between clone cells mildly reduced the rate of apical delamination but was not sufficient to prevent clone splitting (Fig. 6H, movieS3). However, in the flat epithelium, maintaining cell-cell adhesion between clone cells, together with **Ai** occurring, led to a complete reversal of the directionality of delamination (Fig. 6H, movieS3). To further implement adhesion between clone cells, we added a maximum distance rule between clone cells such that upon detachment from the matrix (**B**) clone cells are prevented from drifting away from each other, mimicking maintenance of a strong lateral adhesion. This did not affect the outcome of the simulations in the flat epithelium (Fig. 6I, movie S4). By contrast, in the pseudostratified tissue, enforcing lateral adhesion suppressed clone splitting and made apical delamination a rare case (Fig. 6I, movieS4).

*In vivo*, delamination occurs while E-cad is still detected in clone cells suggesting that adhesion between clone cells and control cells may not systematically be lost. Therefore, we also tested alternative scenarios in which only events **ApC** and **B** occur (Fig. 6 JK). In the flat tissue, the maintenance of adhesion between mutant and wild-type cells made apical delamination the main outcome. In the pseudostratified epithelium, the overall delamination rate is progressively reduced as clone size increases and the apical delamination, which was a rare event in the **ApC Ai B** scenario, now represents a third of all outcomes.

### **Basal membrane rigidity regulates directionality of delamination exclusively in the flat epithelium**

*In vivo*, all events seem to occur in a relatively short time window (circa 3-4h). Therefore, we decided to implement various scenarios in the pseudostratified epithelium allowing events to take place within a 4h time frame (Fig. S5 A-D). Rushing cells to perform the various events did not affect the overall outcome of each tested scenario. Next, we tested an extreme case with **A** and **B** occurring simultaneously in each epithelium (Fig. S5E). Again, in the pseudostratified epithelium the effect is marginal as basal delamination dominates. However, in the flat tissue having **A** and **B** implemented simultaneously randomizes delamination in single cells and slightly favors basal delamination in larger clones (Fig. S5E).

These simulations indicate that epithelial destabilization in the short pseudostratified tissue primarily leads to basal delamination with marginal effects from the order and timing of events. They also show that extensive cell-cell adhesion (apical and lateral) is required for delamination to occur collectively. By contrast, in the flat epithelium, epithelial destabilization in a single cell preferentially leads to apical delamination but the tissue is highly sensitive to the type of events taking place, in which order they occur and to clone size. For instance, modulating adhesion between clone cells or between clone cells and control cells was sufficient to toggle between apical and basal delamination.

So far, all simulations were run in a permissive context in which the basal compartment does not act as a physical barrier. However, *in vivo*, both flat and pseudostratified layers of the eye-antennal disc are anchored to an extracellular matrix. To test the impact of such environment, we assessed the outcomes of some of the previously tested scenarios in the context of a non-permissive basal matrix acting as a physical obstacle and as a substrate, forcing cells to experience a small degree of confinement (Fig. 7A-C, movieS5). As expected the non-permissive matrix prevents basal delamination. Interestingly, in the flat tissue, this was sufficient to promote apical delamination for all scenario including the ones that have an intrinsic bias towards basal delamination (Fig. 7A, compared to Fig. 6I). However, in the pseudostratified epithelium preventing basal delamination is not sufficient to drive apical delamination (Fig. 7A-C). To assess whether the non-permissive matrix nonetheless influenced the position of clone cells in the pseudostratified tissue, we monitored the rate of basal positioning which indicates the percentage of cells with their nuclei located in a more basal position than the average position of the control cells (Fig. 7D, E). Interestingly, all scenarios tested in the pseudostratified epithelium led to basal positioning of cells (Fig. 7E). This indicates that the intrinsic basal directionality induced by epithelial destabilization observed in the pseudostratified tissue still occurs despite actual delamination being prevented by the non-permissive matrix. Overall, in the flat epithelium there are various possible outcomes of epithelial destabilization depending on the type and order of events but these are likely to be cancelled by the presence of the matrix acting as a physical barrier which strongly biases delamination towards the apical side. By contrast, all scenarios tested in the pseudostratified tissue led to basal accumulation of cells that either delaminate if the matrix is permissive or remain in the tissue if the matrix acts as a physical barrier.

### **Mechanical forces and preferential adhesion are at interplay during apical collective delamination of tumors**

Mathematical modelling of epithelial destabilization in a flat tissue revealed loss of adhesion between mutant cells and wild-type neighbors is sufficient to revert the directionality of apical delamination despite mutant cells showcasing preferential adhesion. Counterintuitively, this suggests that intraconal adhesion between mutant cells and intercellular adhesion with wild-type neighbors are required to elicit apical collective delamination out of a flat epithelium. *In silico* results coincided with *in vivo* observations and noted apical constriction to be an important feature during collective delamination. To gain more insight on the underlying mechanisms of apical collective delamination, we studied the activation of the actomyosin cytoskeleton network, using phospho-Myo as a proxy, together with junctional markers. As aforementioned, during early apical collective delamination, clones underwent apical constriction and clustered in a dome-like shape (Fig. 8A). Mutant cells were embedded in the cell layer and emitted apical lumen protrusion, hence the term “octopus” to describe this stage. Phospho-Myosin was enriched at the periphery of the octopus, at the interface between mutant clones and their wild-type counterparts (Fig. 8B, yellow arrows). We also observed cytoskeleton remodeling at the tip of lumen protrusions (Fig. 8B yellow and green arrowheads), suggesting both non-cell autonomous and cell-autonomous forces were at play early during apical collective delamination events. During metamorphosis of the pupal abdomen, an extracellular ring of actomyosin forms non-cell autonomously to extrude larval epidermal cells (Teng et al., 2017). This supracellular structure has also been described as part of the tissue clearance mechanisms used to eliminate the epidermal cells of the pupal notum, which eventually extrude and die by apoptosis (Villars et al., 2022). However, no caspase activation was detected at the octopus stage (Fig. 8C), suggesting apical collective

delamination occurs independently of caspase-activation and involved cytoskeleton remodeling at the periphery of mutant cells. Mathematical modelling ~~also~~ revealed that lateral adhesion between mutant and wild-type cells was essential for collective apical delamination in a flat epithelium. At later stages of apical collective delamination, when cells collectively translocated in the lumen, we observed *in vivo* a ring-like structure enriched in adhesion proteins like Coracle and E-cad (Fig. 8D, E, blue arrows). We termed this structure the neck, through which cells left the flat epithelium and delaminated, translocating their nucleus and cytoplasm into the lumen (Fig. 8D, E, blue arrowhead). Three-dimensional reconstruction and quantification revealed the neck to be on average 3 $\mu$ m in diameter (Fig. 8F). This value is in range with *in vivo* studies cell migration of dendritic cells in the mouse ear skin, for which a minimal diameter of 2 $\mu$ m suffices (Raab et al., 2016). Altogether, our *in silico* and *in vivo* results suggest tumors with disrupted SJ integrity undergo basal collective delamination when originated in a pseudostratified epithelium regardless of the order of junctional remodeling. Conversely, SJ-deficient tumors formed in a flat epithelium exclusively undergo apical collective delamination. Moreover, the directionality of collective delamination in flat epithelia is highly to the sequence in which junctional remodeling is orchestrated and preferential adhesion between mutant cells, and to their wild-type neighbors ensures collectiveness and completion of the process.

## Discussion

### **SJ loss promotes cell elimination in the larval eye disc**

Here, using an *in vivo* cooperative tumorigenesis system in the *Drosophila* larval eye disc, we found that loss of SJ integrity alone can trigger caspase-induced elimination during L2 and L3 stages. This elimination takes place before the developmentally programmed cell-death occurs during pupal metamorphosis (Wolff & Ready, 1991). Hence, SJ-deficient clones are removed from the eye independently of this process. SJ play a major role in the establishment of the blood-retinal-barrier, sealing light-sensitive photoreceptors from the circulating hemolymph to enable phototransduction (Banerjee et al., 2008). Our results reveal single mutant cells deficient for bi- or tri-cellular SJ are prone to die by apoptosis in the flat and pseudostratified epithelium. We reasoned this could be due to cell competition mechanisms, known to preserve tissue homeostasis by removing potentially hazardous cells from the cell layer (Baker, 2020; Levayer, 2018; Morata, 2021). Loss of SJ integrity could decrease the relative fitness of mutant cells in comparison to their adjacent wild-type neighbours due to changes in the molecular fitness fingerprints or mechanical properties. This would in turn trigger cell competition and promote the elimination of SJ mutant cells via caspase-activation. At the molecular level, loss of fitness in mutant cells could be due to the mislocalization of SJ components. In the pupal notum, disruption of bicellular SJ upon loss of *nrv2* leads to a spreading of Gli from tricellular SJ into the bicellular SJ domain (Esmangart de Bournonville & Le Borgne, 2020). In the wing disc which, Gli mislocalization promotes Dlg downregulation and ultimately triggers cell elimination (Padash-Barmchi et al., 2010, 2013). Alternatively, loss of SJ integrity in the eye disc could be accompanied by the dysregulation of the ESCRT/retromer system, as described in the pupal notum (Esmangart de Bournonville et al., 2024). This would result in the accumulation of ubiquitinated substrates and proteotoxic stress, triggering cell competition as observed in the wing disc (Baumgartner et al., 2021). Furthermore, differences in the rate of proliferation between two cell populations in

a mosaic tissue triggers cell competition and elimination of the slower cycling population (Morata & Ripoll, 1975). Cora was first identified as a dominant negative suppressor of the Epidermal Growth Factor Receptor (EGFR) signaling pathway responsible for promoting cell survival (Fehon et al., 1994). *cora* loss-of-function decreases cell proliferation, triggering cell elimination in the eye-antenna and wing imaginal discs without causing major tissue disruption (Ward et al., 2001).

### **Cooperative SJ loss and oncogenic Ras promote collective delamination of living**

Strikingly, our findings show that upon loss of SJ in cooperation with Ras malignant transformation, SJ-deficient tumors do not die. Instead SJ-deficient tumors undergo different types of collective cell movements, namely tissue folding and apical or basal collective delamination of living cells. This is, to our knowledge, one of the first descriptions of a permissive function for SJ together with oncogenic Ras in the initiation of cell delamination. We reasoned Ras overactivation in SJ-depleted cells bestows a fitness advantage and masks the “loser” fitness status. This would in turn transform SJ-mutant *Ras*<sup>V12</sup> cells in “super-competitors”, a phenomenon observed in the context of tumor progression (Cong & Cagan, 2024). Ras overactivation in the wing disc does not generate significant overgrowth but instead upregulates the oncogene *dMyc*, rendering cells refractory to apoptosis due to the ectopic trans-activation of *head involution defective (hid)* by the Ras-MAPK pathway (De La Cova et al., 2004; Moreno & Basler, 2004; Pinal et al., 2018). Ras overactivation in the eye disc also downregulates *hid*, promoting cell survival (Bergmann et al., 1998) while *Ras*<sup>V12</sup> transformed cells trigger compaction and elimination wild-type neighbors in the pupal notum (Levayer et al., 2016; Moreno et al., 2019).

### **Folding morphogenesis exhibits preferential cell adhesion mediated by E-cadherin and $\beta$ -integrin**

We performed spatiotemporal characterization and dissected the cellular steps of collective cell movements elicited by SJ-deficient *Ras*<sup>V12</sup> tumors. Our results show tissue folds exclusively form in the pseudostratified epithelium of the eye disc. This tissue differentiates with the posterior-to-anterior MF progression and is composed of two cell populations: undifferentiated progenitors, anterior to the MF, and differentiated cells, posterior to the MF (Warren & Kumar, 2023). In this epithelium, folding morphogenesis of SJ-deficient *Ras*<sup>V12</sup> tumors comprises junctional remodeling at apical, lateral and basal domains. This mechanical coupling has also been observed in other tissues (Denk-Lobnig & Martin, 2020; Tozluoglu & Mao, 2020). We describe how junctional rearrangements differ depending on cell identity and describe the presence of  $\beta$ -integrin and E-cad-mediated adhesion during tissue folding. Firstly, Elav-negative SJ-depleted *Ras*<sup>V12</sup> tumors anterior to the MF exhibit a partial loss of polarity and undergo apical constriction. Concomitantly the lateral cortex is remodeled, evidenced by E-cad spreading and P-Myo enrichment, while focal adhesions preserve basal anchoring to the extracellular matrix. Basolateral enrichment of the phosphorylated regulatory light chain of non-muscle type II myosin (P-Myo) suggests an increase in contractility of the actomyosin cytoskeleton at this cortical domain (Fox & Peifer, 2007; Mao et al., 2013). The partial loss of polarity and junctional remodeling events persist, and apical constriction continues. Moreover, tissue folds appear enriched in the focal adhesion component  $\beta$ -integrin at apical and lateral domains. This suggests the presence of

preferential adhesion mediated by E-cad and  $\beta$ -integrin. In *Xenopus*, during the migration of neural crest cells, cadherins have been found to function at focal adhesion and mediate adhesion to the extracellular matrix (Langhe et al., 2016). It would be interesting to further explore whether integrins can also reciprocate and function to mediate intercellular adhesion. E-cad homotypic interaction is well studied (Brasch et al., 2012) and could be reinforced by the not so well understood homo-oligomerization of  $\beta$ -integrin  $\alpha$ -chains, a thermodynamically favorable process previously described in MDCK cells (Manninen, 2015; Maurer et al., 2002; Mehrbod & Mofrad, 2013). In striking contrast, clones located posterior to the MF do not showcase E-cadherin lateral localization at any point during the sequence of junctional remodeling events. SJ-depleted *Ras*<sup>V12</sup> tumors posterior to the MF are Elav-positive and appear well polarized. Tissue folding in these clones starts with the constriction of the apical domain and simultaneous loss of basal anchoring to the extracellular matrix. As apical constriction progresses and the epithelium invaginates, basal loss of  $\beta$ -integrin is concomitant to the specific enrichment or relocalization of  $\beta$ -integrin at the apical domain of mutant cells. This reinforces the notion that strengthening cell-cell adhesion via interplay of E-cad and  $\beta$ -integrin-mediated adhesion may be essential for tissue folding. We cannot rule out the possibility that extracellular matrix may be present at this location, in which case E-Cad and  $\beta$ -integrin could cooperate to provide adhesion, as seen in the *Xenopus* neural crest (Langhe et al., 2016). However, interplay between E-Cad and  $\beta$ -integrin adhesion modules independently of extracellular matrix has been observed *in vitro* during mitosis in cultured cells (Huber et al., 2023). This interplay has also been reported *in vivo*, during embryonic dorsal closure (Narasimha & Brown, 2004) and basal tissue folding of the pseudostratified epithelium in the wing disc (Valencia-Expósito et al., n.d.). Our results further highlight the complexity of tissue folding in pseudostratified epithelia and reveal striking differences of  $\beta$ -integrin and E-cad remodeling concomitant to cell identity and polarity status. The small GTPase Rap1 regulates Cadherin- and Integrin-based adhesion modules during morphogenesis (Boettner & Van Aelst, 2009). During mesoderm invagination in the embryo, Rap1 acts together with Canoe, an adherens junctions-cytoskeleton linker, and regulates  $\beta$ -integrin and E-cad localization (McMahon et al., 2010; Sawyer et al., 2009; Vale et al., 2023). In the eye disc, posterior to the MF, Rap1 affects Notch and EGFR signaling. Rap1 acts through Canoe to regulate E-cad and Baz levels in ommatidia, controlling cell specification and retinal morphogenesis (Gaengel & Mlodzik, 2003; O’Keefe et al., 2009; Walther et al., 2018; Yost et al., 2023). Anterior to the MF, Wingless (Wg) controls the speed of MF progression, which also depends on the expression of integrins by Hedgehog (Hh) and Decapentaplegic (Dpp) signaling. In the wing disc, wg governs tissue folding by basally stabilizing integrins. Hence, the molecular mechanisms regulating folding morphogenesis may be subjected to tissue-intrinsic properties and developmental programs.

### **Collective delamination of living cells requires preferential adhesion mediated by E-cadherin and $\beta$ -integrin**

Furthermore, SJ-deficient *Ras*<sup>V12</sup> cells delaminate collectively and alive out of an epithelium, either apically or basally. We have dissected the cellular steps and regulators of the collective delamination of living cells. Our experimental and theoretical results highlight the choice of directionality during delamination is not random, but is instead governed by tissue architecture and preferential cell adhesion. We put forward a detailed molecular plan of junctional remodeling taking place during collective delamination of live tumors. Basal collective delamination of living cells occurs exclusively in the pseudostratified epithelium

regardless of the sequence in which junctional complexes are remodeled. This results in the formation of Elav-positive polarized rosettes, radially organized and apically enriched in E-cad, F-actin and  $\beta$ -integrin. We find striking similarities in terms of cell identity, cluster size and remodeling of junctions and the cytoskeleton between rosettes and apically constricted SJ-deficient tumors posterior to the MF. Live imaging will be decisive to unambiguously determine whether rosettes originate indeed posterior to the MF. Conversely, SJ-deficient tumors in the flat epithelium solely undergo apical collective delamination alive out of the epithelium and the sequence of events greatly impacts the directionality of delamination. Our results confirm the synergy between M6 depletion and  $Ras^{V12}$  in promoting cell delamination reported on a previous study (Dunn et al., 2018). Dunn and colleagues identified JNK signaling and Canoe induction of cell-autonomous MyoII contractility via Rho1 activation as mechanical regulators of apical collective delamination (Dunn et al., 2018). The aforementioned study did not include a detailed characterization for the epithelial origin of cells undergoing apical collective delamination. However, they reported clones in the pseudostratified epithelium deviate apically, a phenotype never observed in the experimental set up and analyses conducted in the present study. We performed a detailed spatiotemporal characterization of apical and basal collective delamination and studied markers of junctional and cytoskeletal remodeling, cell identity and polarity status. Larvae were staged from L2 until L3 with a 2h-time window that overlapped across replicates, covering a maximum time of larval development from 76h to 120h. The reported duration of apical collective delamination in (Dunn et al., 2018) was of 190h minutes. Hence, it is unlikely any event of apical or basal collective delamination to have been underscored in our analyses. We quantified nuclear size in clones from the flat and pseudostratified epithelium and compared it to the nuclear size of apically deviated clones. Nuclear size of clones having undergone apical deviation is reminiscent to that of clones from the flat epithelium, which is significantly bigger than clones in the pseudostratified layer. Moreover, we performed mathematical modeling using a powerful EMT-simulator adapted to the eye disc architecture. Both *in vivo* and *in silico* results reveal apical collective delamination events exclusively originate from the flat epithelium, and never from the pseudostratified one. The reason for the discrepancy between the origin of apically delaminating clones between the aforementioned study (Dunn et al., 2018) and our results remains unknown. Live imaging with clonal and junctional markers would help clarify this issue. In any case, our studies expand on the role of bi- and tricellular SJ components and we report a non-occluding function of SJ in preventing cell extrusion in the eye disc. Loss of SJ integrity synergizes with oncogenic Ras and promotes collective delamination of tumors alive out of the epithelium.

Collective apical delamination in the flat epithelium starts with SJ-deficient  $Ras^{V12}$  tumors acquiring a dome-like shape and forming an “octopus”. Basolateral preferential adhesion between mutant cells is mediated by E-cad and  $\beta$ -integrin. At the apical domain, cell protrusions are emitted in the lumen. Concomitantly, an apical neck is formed and contains Cora and E-cad. Mutant cells delaminate collectively and alive out of the flat tissue through this neck, deviating in the lumen while remaining cohesive. The presence of P-Myo and phalloidin at the tip of apical lumen protrusions suggests the SJ-deficient tumor could exert pulling forces at the end of cell protrusions. In addition, P-Myo is enriched at the lateral pole, all along the rim of the SJ-deficient tumor, forming what looks like a supracellular cable. The contraction of such supracellular cable could exert pushing forces that would in turn contribute to apical delamination. This supracellular cable could be formed by wild-type neighbors, as observed during cell extrusion in the pupal abdomen and notum (Levayer et



al., 2016; Teng et al., 2017). Importantly, *in silico* mathematical modelling of the flat epithelium highlights cell adhesion between wild-type and mutant cells to be essential for apical collective delamination. This suggests E-cad mediated apical adhesion observed *in vivo* at the neck is key for this process. The relative contribution of mechanical forces in this process awaits further studies. Yet, cell-autonomous pulling forces could be exerted at the tip of apical lumen protrusions concurrent to non-cell autonomous pushing forces located at the mutant-wild-type interface of the actomyosin supracellular cable. Our study hence suggests mechanical tension exerted by neighbors may not be restricted to apoptotic-dependent cell extrusion (Villars & Levayer, 2022). Therefore, non-cell autonomous forces may be required for apical collective delamination of living cells. It would be very informative to prevent force activation cell-autonomously in mutant cells or non-cell-autonomously in wild-type neighbors to further elucidate their contribution to this process. Moreover, studying actomyosin force regulators such as  $\alpha$ -catenin, fluorescently tagged and expressed exclusively in the mutant or wild-type cells, would clarify the source of mechanical activation and force generation. This would clarify whether supracellular myosin cables form exclusively during caspase-dependent cell extrusion or whether this mechanism is overridden by “super-competitor” tumors and required for living cells to delaminate collectively. Tumor delamination is the first step in metastasis onset. Further characterization of the molecular regulators involved may shed light on ubiquitous mechanisms required for collective cell rearrangements and co-opted by cancer cells to drive tumor malignancy. Moreover, the direction in which cells leave an epithelium can be critical for determining cell fate (Gu & Rosenblatt, 2012). TJ in vertebrates, the somewhat analogous to invertebrates’ SJ, are located apical to adherens junctions. Oncogenic transformation triggers basal extrusion, with cancerous cells leaving the epithelium from the membrane side farthest to the TJ domain. Interestingly, our results show SJ-depleted *Ras*<sup>V12</sup> tumors in *Drosophila* leave the flat epithelium apically, also through the cell pole farthest away from SJ. Further studying apical collective delamination in *Drosophila* could help identify conserved molecular regulators involved in vertebrate basal extrusion. Moreover, live delamination is the first step in cancer metastasis and epithelia to mesenchymal (EMT) transition (Yang et al., 2020). Classical EMT hallmarks such as the switch from E-cad to N-cadherin have been revisited. Novel studies show this step is not required for EMT, but rather comprises one of the many possible EMT states (Font-Noguera et al., 2021; Yang et al., 2020). Similarly, initially thought to be a hallmark for EMT, E-cad loss is not required for EMT onset. In some EMT scenarios, E-cad is not lost at all, but instead E-cad remodeling appears tightly regulated across time (Acloque et al., 2024; Campbell & Casanova, 2015; Font-Noguera et al., 2021). Similarly, transcription factors involved in EMT during gastrulation such as Snail and Twist are not implicated in every apical constriction event of EMT, namely single cell delamination during neuroblast ingression (An et al., 2017; Sidor & Röper, 2017; Simões et al., 2017). These observations coincide with our results of persistence of cell-cell adhesion during the collective delamination of living cells via E-cad and  $\beta$ -integrin mediated adhesion. Hence, the cellular steps of collective delamination of living cells identified in this study may occur during EMT onset. Finally, tricellular and bicellular SJ core-components found to synergize with Ras and trigger EMT onset in this study appear frequently mutated in several types of carcinoma. This further cements the role of cell junctions in tumor dissemination (Kyuno et al., 2021).

The experimental findings reported here have direct implications in understanding the cellular steps of the collective delamination of living cells *in vivo*. Moreover, the mathematical framework described here provide insights into how tissue architecture and preferential cell

adhesion govern the directionality of delamination, which ultimately determines cell fate, a deeply fundamental question in developmental and cancer biology. Ultimately, we expect our work to help understand how apical and basal collective delamination of living cells differ from each other in terms of junctional remodeling, cell polarity and cell identity, and the underlying mechanism governing directionality in both normal and pathological conditions.

## Materials and methods

### Experimental model

All *Drosophila* stocks were maintained on media consisting of corn meal, sugar, yeast, and agar on incubators at a constant temperature of 25°C.

### *Drosophila* genotypes

#### Figure 1

**B, C-  $M6^{(W18Stop)}$ , FRT79E eyMARCM** obtained by crossing *yw*, *eyFlp*; *act-Gal4*, *UAS-nls::GFP*; *tub>Gal80*, *FRT79E* / with ; *lf* / *CyO*;  $M6^{(W18Stop)}$ , *FRT79E* / *TM6*, *Tb*, *Hu*

**E, F-  $UAS-Ras^{V12}$ ;  $M6^{(W18Stop)}$ , FRT79E eyMARCM** obtained by crossing *yw*, *eyFlp*; *act-Gal4*, *UAS-nls::GFP*; *tub>Gal80*, *FRT79E* / with ; *UAS-Ras<sup>V12</sup>*;  $M6^{(G152)}$ , *FRT79E* / *TM6*, *Tb*, *Hu*

#### Figure 2

**B, C, E, F, H, I-  $UAS-Ras^{V12}$ ;  $M6^{(W18Stop)}$ , FRT79E eyMARCM** obtained by crossing *yw*, *eyFlp*; *act-Gal4*, *UAS-nls::GFP*; *tub>Gal80*, *FRT79E* / with ; *UAS-Ras<sup>V12</sup>*;  $M6^{(G152)}$ , *FRT79E* / *TM6*, *Tb*, *Hu*

#### Figure 3

**B, C, E, F-  $aka^{L200}$ , FRT40A;  $UAS-Ras^{V12}$ ; eyMARCM** obtained by crossing *hsFlp*, *act-Gal4*, *UAS-nls::GFP/FM6*; *ptub-Gal80*, *FRT40A* / *CyO* with ;  $aka^{L200}$ , *FRT40A*; *UAS-Ras<sup>V12</sup>* / *SM5* – *TM6*, *Tb*, *Hu*

#### Figure 4

**B, D, F, H-  $UAS-Ras^{V12}$ ;  $M6^{(W18Stop)}$ , FRT79E eyMARCM** obtained by crossing *yw*, *eyFlp*; *act-Gal4*, *UAS-GFP*; *tub>Gal80*, *FRT79E* / with ; *UAS-Ras<sup>V12</sup>*;  $M6^{(G152)}$ , *FRT79E* / *TM6*, *Tb*, *Hu*

**J-  $aka^{L200}$ , FRT40A;  $UAS-Ras^{V12}$ ; eyMARCM** obtained by crossing *hsFlp*, *act-Gal4*, *UAS-nls::GFP/FM6*; *ptub-Gal80*, *FRT40A* / *CyO* with ;  $aka^{L200}$ , *FRT40A*; *UAS-Ras<sup>V12</sup>* / *SM5* – *TM6*, *Tb*, *Hu*

#### Figure 5

**B, E, F, H-  $UAS-Ras^{V12}$ ;  $M6^{(W18Stop)}$ , FRT79E eyMARCM** obtained by crossing *yw*, *eyFlp*; *act-Gal4*, *UAS-GFP*; *tub>Gal80*, *FRT79E* / with ; *UAS-Ras<sup>V12</sup>*;  $M6^{(G152)}$ , *FRT79E* / *TM6*, *Tb*, *Hu*

**C, I- *glij<sup>DV3</sup>*, FRT40A; UAS-*Ras<sup>V12</sup>* ; eyMARCM** obtained by crossing *hsFlp*, act-Gal4,UAS-nls::GFP/FM6 ; ptub-Gal80, FRT40A / CyO with ; *glij<sup>DV3</sup>*, FRT40A; UAS-*Ras<sup>V12</sup>* / SM5 – TM6, Tb, Hu

### Figure 8

**B, C, E, - UAS-*Ras<sup>V12</sup>* ; *M6<sup>(W18Stop)</sup>*, FRT79E eyMARCM** obtained by crossing yw, eyFlp ; act-Gal4, UAS-GFP ; tub>Gal80, FRT79E / with ; UAS-*Ras<sup>V12</sup>* ; *M6<sup>(G152)</sup>*, FRT79E / TM6, Tb, Hu

### Supplementary Figure 1

**B- *M6<sup>(W18Stop)</sup>*, FRT79E eyMARCM** obtained by crossing yw, eyFlp ; act-Gal4, UAS-GFP ; tub>Gal80, FRT79E / with ; If / CyO ; *M6<sup>(W18Stop)</sup>*, FRT79E / TM6, Tb, Hu

**C, D- *aka<sup>L200</sup>*, FRT40A eyMARCM** obtained by crossing *hsFlp*, act-Gal4, UAS-nls::GFP/FM6 ; ptub-Gal80, FRT40A / CyO with ; *aka<sup>L200</sup>*, FRT40A; MKRS / SM5 – TM6, Tb, Hu

**E, F- *nrv2<sup>K13315</sup>*, FRT40A eyMARCM** obtained by crossing *hsFlp*, act-Gal4,UAS-nls::GFP/FM6 ; ptub-Gal80, FRT40A / CyO with; *nrv2<sup>K13315</sup>*, FRT40A; If / SM5 – TM6, Tb, Hu

### Supplementary Figure 2

**B,C- UAS-*Ras<sup>V12</sup>* ; *M6<sup>(W18Stop)</sup>*, FRT79E eyMARCM** obtained by crossing yw, eyFlp ; act-Gal4, UAS-GFP ; tub>Gal80, FRT79E / with ; UAS-*Ras<sup>V12</sup>* ; *M6<sup>(G152)</sup>*, FRT79E / TM6, Tb, Hu

**E, F- *aka<sup>L200</sup>*, FRT40A; UAS-*Ras<sup>V12</sup>* ; eyMARCM** obtained by crossing *hsFlp*, act-Gal4,UAS-nls::GFP/FM6 ; ptub-Gal80, FRT40A / CyO with ; *aka<sup>L200</sup>*, FRT40A; UAS-*Ras<sup>V12</sup>* / SM5 – TM6, Tb, Hu

**G,H- *nrv2<sup>K13315</sup>*, FRT40A; UAS-*Ras<sup>V12</sup>* eyMARCM** obtained by crossing *hsFlp*, act-Gal4,UAS-nls::GFP/FM6 ; ptub-Gal80, FRT40A / CyO with; *nrv2<sup>K13315</sup>*, FRT40A; If / SM5 – TM6, Tb, Hu

### Supplementary Figure 3

**B, D, F, H, J,- UAS-*Ras<sup>V12</sup>* ; *M6<sup>(W18Stop)</sup>*, FRT79E eyMARCM** obtained by crossing yw, eyFlp ; act-Gal4, UAS-GFP ; tub>Gal80, FRT79E / with ; UAS-*Ras<sup>V12</sup>* ; *M6<sup>(G152)</sup>*, FRT79E / TM6, Tb, Hu

**K- *aka<sup>L200</sup>*, FRT40A; UAS-*Ras<sup>V12</sup>* ; eyMARCM** obtained by crossing *hsFlp*, act-Gal4,UAS-nls::GFP/FM6 ; ptub-Gal80, FRT40A / CyO with ; *aka<sup>L200</sup>*, FRT40A; UAS-*Ras<sup>V12</sup>* / SM5 – TM6, Tb, Hu

### Larvae staging

Flies were crossed and flipped ~48h after initial crossing to stage larvae using as reference the number of hours after egg laying (h AEL). A 2h interval was left after the flip to allow for egg deposition, taking this time point as the “0h AEL” reference.

### Immunostaining and image acquisition

Eye-antenna imaginal discs from staged larvae were dissected and fixed for 15min in 4% formaldehyde & permeabilized/washed in PBT 0.1%, stained with primary antibody solution

for 3h at RT, washed and then stained overnight with secondary antibody solution & DAPI (0.5mg/mL, 1:1000 dilution) at 4°C. The antibodies used are detailed in the Key Resources Table. Dissected imaginal discs were mounted in 0,5% N-propylgallate dissolved in 90% glycerol/PBS 1X final & imaged on a Leica inverted confocal SP8 or a Leica upright confocal SPE using a 10X (N.A. 0.3) air objective and oil immersion objectives 20X (N.A. 0.7) & 63X (N.A. 1.4). Images were acquired using a 405 laser to excite DAPI stain and detected with a hybrid detector (HyD). A 488 nm argon laser used to excite the GFP fluorophore, endogenously expressed under the UAS and detected with a HyD. A 561nm DPSS diode laser used to excite Cy-3, detected with a HyD. A 633nm DPSS diode laser used to excite Cy-5 and detected with a photomultiplier tube (PMT4).

### Image processing and analysis

All image processing and analysis was performed using Fiji. For immunofluorescence and fluorescent reporter microscopy-based assays, all measurements were derived from the eye part of the eye-antenna imaginal disc.

### Measuring distance to the morphogenetic furrow

High and low magnification confocal microscopy images were used to measure the distance from the cell in the clone closer to the forefront of the MF, identified at the most posterior apically constricted apex in the tissue indentation of the pseudostratified epithelium. Measurements were carried out for clones in each of the events of tissue fold anterior to the MF (no difference with wild-type counterparts, apical constriction, tissue invagination) and posterior to the MF (apical constriction, tissue invagination) as well as step of apically delaminating clones (octopus, transition in the lumen, clone detachment).

### Quantification of clone size during collective delamination and tissue formation

Confocal microscopy images of *Drosophila* heterozygous eye-antennal imaginal discs immuno-stained with anti-E-cad (grey) and anti-phosphorylated histone 3 (PH3) or Cleaved-Casape-3 (C-Cas3) were analyzed. Clone size was quantified by counting the number of nuclei in the clones of SJ-deficient *Ras*<sup>V12</sup> transformed cells, expressing the GFP clone marker. Clone size for each step of apical and basal collective delamination and tissue formation was quantified and average size of clone cluster was obtained.

### Computational modelling

The model has been modified from a previously published model (Plunder et al 2024). Briefly, cells are abstracted to nuclei attached to a set of adjustable springs connecting them to an apical point and a basal point. Apical points of adjacent cells are also attached by springs. Basal points are attached to a simple non-deformable basal line representing the basement membrane. Nuclei repel each other via a repulsion force acting on their soft outer cores. The hard inner cores of nuclei cannot overlap. Loss of apical or basal adhesion (events **A** and **B**) remove the adjustable apical-nuclei or basal-nuclei springs. The new event **ApC** increases the strength of the strings between adjacent apical points for clone cells. Parameters were adapted to allow flat and short pseudostratified configurations to emerge. The transition between pseudostratified and flat epithelial epithelium is achieved by changing a limited set of parameters (Supplementary Table 1). For instance, the allowed maximal distance between basal points. When set to 10  $\mu\text{m}$  this distance allows cells to arrange themselves as a flat monolayer. When set to 3  $\mu\text{m}$  it forces cells to redistribute their nuclei

along the apicobasal axis to minimize tension/compression and this generates pseudostratification. To prevent the pseudostratified tissue from growing over 3-4 pseudolayers a maximum height is set and acts as a constraint. Since by default the basal compartment located below the basal line is permissive and does not act as a physical obstacle, the flat tissue tends to flip and rotate around the basal line. To prevent this behavior, we added a very weak repulsive within the basal compartment which pushes cells weakly upwards as soon as a nucleus is below the basal line, the strength of this force is 2.5 % of the nuclei-nuclei repulsion force strength and does not prevent basal delamination. For simulations with non-permissive matrix we tuned this force to 250 % of the nuclei-nuclei repulsion force. Further modification of the model includes a new event called **Ai**. During this event, the apical-apical springs at the interface between control cells and clone cells are removed and a recovery phase is added where the two disconnected apical layers of control cells directly connect again with a long apical-apical spring crossing the gap caused by the intermediate EMT cells. The rest length of this apical-apical spring goes to zero with a constant speed of 5 $\mu$ m/h. Montage of simulation outputs into supplementary movies was made using VSDC video editor.

### Key resources table

REAGENT or RESOURCE	SOURCE	IDENTIFIER
Antibodies		
Mouse anti- $\beta$ -Integrin (1:250)	DSHB	Cat#CF.6G11; RRID:AB_528310
Mouse anti-Cora (1:200)	DSHB	Cat#C615.16; RRID: AB_116164 4
Mouse anti-Elav (1:200)	DSHB	Cat#9F8A9 ; RRID:AB_528217
Rat anti-DE-cad (1:250)	DSHB	Cat#DCAD2; AB_528120
Mouse anti-Cleaved caspase-3 (1:1000)	Cell Signalling Technology	Cat#Asp175, RRID:AB_2341188
Mouse anti-Phospho-histone H3 (1:1000)	Cell Signalling Technology	Cat#Ser10 (6G3); RRID:AB_331748
Phospho-Myosin Light Chain 2 (1:250)	Cell Signalling Technology	Cat#Ser19; RRID:AB_2250969
Rabbit anti-Cleaved Drosophila Dcp-1 (1:100)	Cell Signalling Technology	Cat#Asp215; RRID:AB_2721060
Mouse anti-Gli (1:100)	(Auld et al., 1995)	Cat#1F61D4 [48]
Alexa Fluor™ 647 Phalloidin (1:1000)	Thermo Fisher Scientific	Cat#A22287
Rabbit anti-aPKC (1:500)	Santa Cruz Biotechnology	Cat# sc-208; RRID:AB_2168668

DAPI 4',6-diamidino-2-phenylindole (1:1000)	Thermo Scientific	Fisher	Cat# D1306, RRID:AB_2629482
Chemicals, peptides, and recombinant proteins			
Paraformaldehyde	EMS		19340-72
Triton X-100	Euromedex		2000B
Phosphate Buffered Saline	Lonza		BE17-515F
Deposited data			
<i>D.melanogaster</i> : Aka::GFP <i>D.melanogaster</i> : <i>hsFLP</i> ; <i>aka</i> <sup>L200</sup> , FRT40A / CyO	(Byri et al., 2015) (Esmangart de Bournonville & Le Borgne, 2020)		N/A Gift from Stefan Luschnig
<i>D.melanogaster</i> : <i>Gli</i> <sup>ΔV3</sup> , FRT40A/CyO	(Schulte et al., 2003)		Gift from Vanessa Auld
<i>D.melanogaster</i> : <i>nrv2</i> <sup>DV3</sup> , FRT40A/CyO	(Esmangart de Bournonville & Le Borgne, 2020)		DGRC 114351
<i>D.melanogaster</i> : <i>w</i> ; UAS-Ras <sup>V12</sup> , <i>M6</i> <sup>w186</sup> , FRT79E / TM6, <i>Tb</i> <sup>1</sup> <i>D.melanogaster</i> : <i>hs-FLP</i> ; <i>lf</i> /CyO; <i>M6</i> <sup>w186</sup> , FRT79E / TM6, <i>Tb</i> <sup>1</sup>	(Dunn et al., 2018) (Esmangart de Bournonville & Le Borgne, 2020)		Gift from Tian Xu Gift from Tian Xu
<i>D.melanogaster</i> : <i>yw</i> , <i>eyFLP</i> ; Act > <i>y+Gal4</i> , UAS-GFP; <i>tub-Gal80</i> , FRT79E	(Esmangart de Bournonville & Le Borgne, 2020)		Gift from Tian Xu
<i>D.melanogaster</i> : <i>hsFlp</i> , act-Gal4, UAS-nls::GFP/FM6 ; <i>ptub-Gal80</i> , FRT40A / CyO <i>D.melanogaster</i> : <i>yw</i> , <i>eyFLP</i> ; <i>aka</i> <sup>L200</sup> , FRT40A; MKRS / SM5 – TM6, Tb, Hu	(Perdigoto et al., 2011) This study		N/A
<i>D.melanogaster</i> : <i>yw</i> , <i>eyFLP</i> ; <i>aka</i> <sup>L200</sup> , FRT40A; UAS-Ras <sup>V12</sup> / SM5 – TM6, Tb, Hu	This study		N/A
<i>D.melanogaster</i> : <i>yw</i> , <i>eyFLP</i> ; <i>gli</i> <sup>2DV3</sup> , FRT40A; MKRS / SM5 – TM6, Tb, Hu	This study		N/A
<i>D.melanogaster</i> : <i>yw</i> , <i>eyFLP</i> ; <i>gli</i> <sup>2DV3</sup> , FRT40A; UAS-Ras <sup>V12</sup> / SM5 – TM6, Tb, Hu	This study		N/A
<i>D.melanogaster</i> : <i>yw</i> , <i>eyFLP</i> ; <i>nrv2</i> <sup>K13315</sup> , FRT40A; MKRS / SM5 – TM6, Tb, Hu	This study		N/A
<i>D.melanogaster</i> : <i>yw</i> , <i>eyFLP</i> ; <i>nrv2</i> <sup>K13315</sup> , FRT40A; UAS-Ras <sup>V12</sup> / SM5 – TM6, Tb, Hu	This study		N/A
Fiji (version 2.14.0)	(Schindelin et al., 2012)		<a href="https://imagej.net/Fiji">https://imagej.net/Fiji</a>
Inkscape			<a href="https://inkscape.org/">https://inkscape.org/</a>

Graph Pad Prism 6		<a href="https://www.graphpad.com/">https://www.graphpad.com/</a>
Computational model (source code)	(Plunder et al 2024)	<a href="https://github.com/SteffenPL/sEMTor.jl">https://github.com/SteffenPL/sEMTor.jl</a>
Other		
Confocal Microscope	Leica	LSM TCS SPE, TCS SP5 and TCS SP8

## Acknowledgements

We thank V. Auld, A. Bardin, S. Luschnig, Tian Xu and the Bloomington Stock Center and the National Institute of Genetics Fly Stock Center for providing fly lines. The monoclonal antibodies against Cora, E-cad and  $\beta$ -Integrin were obtained from the Developmental Studies Hybridoma Bank, generated under the auspices of the National Institute of Child Health and Human Development, and maintained by the University of Iowa Department of Biological Sciences. We also thank S Dutertre and X Pinson from the Microscopy Rennes Imaging Center-BIOSIT (France). We are grateful to Chantal Roubinet, Caroline Dillard for critical reading of the manuscript.

## Competing interests

No competing interests declared

## Funding

MMO is supported by Ligue Nationale Contre le Cancer (IP/SC-16639 ) and ARC (ARCD0C42023020006318). SP is supported by the KAKENHI Grant-in-Aid for Early-Career Scientists (Grant number 24K16962). ET is supported by ANR-21-CE13-0028-02 and the Association pour la Recherche contre le Cancer (ARC, ARCPJA22020060002084). RLB is supported by ANR-20-CE13-0015 and ARC (PJA 20191209388)



## References

- Acloque, H., Yang, J., & Theveneau, E. (2024). Epithelial-to-mesenchymal plasticity from development to disease: An introduction to the special issue. *Genesis*, 62(1), e23581. <https://doi.org/10.1002/DVG.23581>
- Amoyel, M., & Bach, E. A. (2014). Cell competition: how to eliminate your neighbours. *Development*, 141(5), 988–1000. <https://doi.org/10.1242/DEV.079129>
- An, Y., Xue, G., Shaobo, Y., Mingxi, D., Zhou, X., Yu, W., Ishibashi, T., Zhang, L., & Yan, Y. (2017). Apical constriction is driven by a pulsatile apical myosin network in delaminating *Drosophila* neuroblasts. *Development (Cambridge)*, 144(12), 2153–2164. <https://doi.org/10.1242/DEV.150763/VIDEO-15>
- Auld, V. J., Fetter, R. D., Broadie, K., & Goodman, C. S. (1995). Gliotactin, a novel transmembrane protein on peripheral glia, is required to form the blood-nerve barrier in *drosophila*. *Cell*, 81(5), 757–767. [https://doi.org/10.1016/0092-8674\(95\)90537-5](https://doi.org/10.1016/0092-8674(95)90537-5)
- Baker, N. E. (2020). Emerging mechanisms of cell competition. *Nature Reviews Genetics* 2020 21:11, 21(11), 683–697. <https://doi.org/10.1038/S41576-020-0262-8>
- Banerjee, S., Bainton, R. J., Mayer, N., Beckstead, R., & Bhat, M. A. (2008). Septate Junctions are Required for Ommatidial Integrity and Blood-Eye Barrier Function in *Drosophila*. *Developmental Biology*, 317(2), 585. <https://doi.org/10.1016/J.YDBIO.2008.03.007>
- Baum, B., & Georgiou, M. (2011). Dynamics of adherens junctions in epithelial establishment, maintenance, and remodeling. *The Journal of Cell Biology*, 192(6), 907–917. <https://doi.org/10.1083/JCB.201009141>
- Baumgartner, M. E., Dinan, M. P., Langton, P. F., Kucinski, I., & Piddini, E. (2021). Proteotoxic stress is a driver of the loser status and cell competition. *Nature Cell Biology* 2021 23:2, 23(2), 136–146. <https://doi.org/10.1038/S41556-020-00627-0>
- Bergmann, A., Agapite, J., McCall, K., & Steller, H. (1998). The *Drosophila* gene *hid* is a direct molecular target of ras-dependent survival signaling. *Cell*, 95(3), 331–341. [https://doi.org/10.1016/S0092-8674\(00\)81765-1](https://doi.org/10.1016/S0092-8674(00)81765-1)
- Boettner, B., & Van Aelst, L. (2009). Control of cell adhesion dynamics by Rap1 signaling. *Current Opinion in Cell Biology*, 21(5), 684–693. <https://doi.org/10.1016/J.CEB.2009.06.004>
- Brasch, J., Harrison, O. J., Honig, B., & Shapiro, L. (2012). Thinking outside the cell: how cadherins drive adhesion. *Trends in Cell Biology*, 22(6), 299–310. <https://doi.org/10.1016/J.TCB.2012.03.004>
- Brumby, A. M., & Richardson, H. E. (2003). scribble mutants cooperate with oncogenic Ras or Notch to cause neoplastic overgrowth in *Drosophila*. *The EMBO Journal*, 22(21), 5769–5779. <https://doi.org/10.1093/EMBOJ/CDG548>
- Buckley, C. E., & St Johnston, D. (2022). Apical–basal polarity and the control of epithelial form and function. *Nature Reviews Molecular Cell Biology* 2022 23:8, 23(8), 559–577. <https://doi.org/10.1038/s41580-022-00465-y>
- Byri, S., Misra, T., Syed, Z. A., Bätz, T., Shah, J., Boril, L., Glashauser, J., Aegerter-Wilmsen, T., Matzat, T., Moussian, B., Uv, A., & Luschnig, S. (2015). The Triple-Repeat Protein Anakonda Controls Epithelial Tricellular Junction Formation in *Drosophila*. *Developmental Cell*, 33(5), 535–548. <https://doi.org/10.1016/j.devcel.2015.03.023>
- Cagan, R. L., & Ready, D. F. (1989). The emergence of order in the *Drosophila* pupal retina. *Developmental Biology*, 136(2), 346–362. [https://doi.org/10.1016/0012-1606\(89\)90261-3](https://doi.org/10.1016/0012-1606(89)90261-3)
- Campanale, J. P., Sun, T. Y., & Montell, D. J. (2017). Development and dynamics of cell polarity at a glance. *Journal of Cell Science*, 130(7), 1201–1207. <https://doi.org/10.1242/JCS.188599>
- Campbell, K., & Casanova, J. (2015). A role for E-cadherin in ensuring cohesive migration of a heterogeneous population of non-epithelial cells. *Nature Communications* 2015 6:1, 6(1), 1–11. <https://doi.org/10.1038/ncomms8998>
- Cong, B., & Cagan, R. L. (2024). Cell competition and cancer from *Drosophila* to mammals. *Oncogenesis* 2024 13:1, 13(1), 1–7. <https://doi.org/10.1038/s41389-023-00505-y>

- De La Cova, C., Abril, M., Bellosta, P., Gallant, P., & Johnston, L. A. (2004). *Drosophila myc* regulates organ size by inducing cell competition. *Cell*, *117*(1), 107–116. [https://doi.org/10.1016/S0092-8674\(04\)00214-4](https://doi.org/10.1016/S0092-8674(04)00214-4)
- Denk-Lobnig, M., & Martin, A. C. (2020). Divergent and combinatorial mechanical strategies that promote epithelial folding during morphogenesis. *Current Opinion in Genetics & Development*, *63*, 24–29. <https://doi.org/10.1016/J.GDE.2020.02.014>
- Despin-Guitard, E., Rosa, V. S., Plunder, S., Mathiah, N., Van Schoor, K., Nehme, E., Merino-Aceituno, S., Egea, J., Shahbazi, M. N., Theveneau, E., & Migeotte, I. (2024). Non-apical mitoses contribute to cell delamination during mouse gastrulation. *Nature Communications* *2024 15:1*, *15*(1), 1–18. <https://doi.org/10.1038/s41467-024-51638-6>
- Dillard, C., Reis, J. G. T., & Rusten, T. E. (2021). RasV12; scrib<sup>-/-</sup> Tumors: A Cooperative Oncogenesis Model Fueled by Tumor/Host Interactions. *International Journal of Molecular Sciences*, *22*(16). <https://doi.org/10.3390/IJMS22168873>
- Duchek, P., & Rorth, P. (2001). Guidance of cell migration by EGF receptor signaling during *Drosophila* oogenesis. *Science (New York, N.Y.)*, *291*(5501), 131–133. <https://doi.org/10.1126/SCIENCE.291.5501.131>
- Dunn, B. S., Rush, L., Lu, J. Y., & Xu, T. (2018). Mutations in the *Drosophila* tricellular junction protein M6 synergize with RasV12 to induce apical cell delamination and invasion. *Proceedings of the National Academy of Sciences of the United States of America*, *115*(33), 8358–8363. [https://doi.org/10.1073/PNAS.1807343115/SUPPL\\_FILE/PNAS.1807343115.SM01.AVI](https://doi.org/10.1073/PNAS.1807343115/SUPPL_FILE/PNAS.1807343115.SM01.AVI)
- Esmangart de Bournonville, T., Jaglarz, M. K., Durel, E., & Le Borgne, R. (2024). ESCRT-III-dependent adhesive and mechanical changes are triggered by a mechanism detecting alteration of septate junction integrity in *Drosophila* epithelial cells. *ELife*, *13*. <https://doi.org/10.7554/ELIFE.91246>
- Esmangart de Bournonville, T., & Le Borgne, R. (2020). Interplay between Anakonda, Gliotactin, and M6 for Tricellular Junction Assembly and Anchoring of Septate Junctions in *Drosophila* Epithelium. *Current Biology*, *30*(21), 4245–4253.e4. <https://doi.org/10.1016/J.CUB.2020.07.090>
- Fehon, R. G., Dawson, L. A., & Artavanis-Tsakonas, S. (1994). A *Drosophila* homologue of membrane-skeleton protein 4.1 is associated with septate junctions and is encoded by the coracle gene. *Development*, *120*(3), 545–557. <https://doi.org/10.1242/DEV.120.3.545>
- Finegan, T. M., Hervieux, N., Nestor-Bergmann, A., Fletcher, A. G., Blanchard, G. B., & Sanson, B. (2019). The tricellular vertex-specific adhesion molecule Sidekick facilitates polarised cell intercalation during *Drosophila* axis extension. *PLoS Biology*, *17*(12). <https://doi.org/10.1371/JOURNAL.PBIO.3000522>
- Flores-Benitez, D., & Knust, E. (2016). Dynamics of epithelial cell polarity in *Drosophila*: how to regulate the regulators? *Current Opinion in Cell Biology*, *42*, 13–21. <https://doi.org/10.1016/J.CEB.2016.03.018>
- Font-Noguera, M., Montemurro, M., Benassayag, C., Monier, B., & Suzanne, M. (2021). Getting started for migration: A focus on EMT cellular dynamics and mechanics in developmental models. *Cells & Development*, *168*, 203717. <https://doi.org/10.1016/J.CDEV.2021.203717>
- Fox, D. T., & Peifer, M. (2007). Abelson kinase (Abl) and RhoGEF2 regulate actin organization during cell constriction in *Drosophila*. *Development*, *134*(3), 567–578. <https://doi.org/10.1242/DEV.02748>
- Gaengel, K., & Mlodzik, M. (2003). Egfr signaling regulates ommatidial rotation and cell motility in the *Drosophila* eye via MAPK/Pnt signaling and the Ras effector Canoe/AF6. *Development*, *130*(22), 5413–5423. <https://doi.org/10.1242/DEV.00759>
- Genova, J. L., & Fehon, R. G. (2003). Neuroglian, Gliotactin, and the Na<sup>+</sup>/K<sup>+</sup> ATPase are essential for septate junction function in *Drosophila*. *The Journal of Cell Biology*, *161*(4), 979–989. <https://doi.org/10.1083/jcb.200212054>
- Germani, F., Bergantinos, C., & Johnston, L. A. (2018). Mosaic Analysis in *Drosophila*. *Genetics*, *208*(2), 473. <https://doi.org/10.1534/GENETICS.117.300256>

- Gudipaty, S. A., & Rosenblatt, J. (2017). Epithelial cell extrusion: Pathways and pathologies. *Seminars in Cell & Developmental Biology*, 67, 132–140. <https://doi.org/10.1016/J.SEMCDB.2016.05.010>
- Guillot, C., & Lecuit, T. (2013). Mechanics of epithelial tissue homeostasis and morphogenesis. *Science*, 340(6137), 1185–1189. [https://doi.org/10.1126/SCIENCE.1235249/SUPPL\\_FILE/GUILLOT.SM.PDF](https://doi.org/10.1126/SCIENCE.1235249/SUPPL_FILE/GUILLOT.SM.PDF)
- Gu, Y., & Rosenblatt, J. (2012). New emerging roles for epithelial cell extrusion. *Current Opinion in Cell Biology*, 24(6), 865–870. <https://doi.org/10.1016/J.CEB.2012.09.003>
- Hall, S., & Ward, R. E. (2016). Septate Junction Proteins Play Essential Roles in Morphogenesis Throughout Embryonic Development in Drosophila. *G3 Genes/Genomes/Genetics*, 6(8), 2375–2384. <https://doi.org/10.1534/G3.116.031427>
- Harris, T. J. C., & Tepass, U. (2010). Adherens junctions: from molecules to morphogenesis. *Nature Reviews Molecular Cell Biology* 2010 11:7, 11(7), 502–514. <https://doi.org/10.1038/nrm2927>
- Higashi, T., Arnold, T. R., Stephenson, R. E., Dinshaw, K. M., Miller Correspondence, A. L., & Miller, A. L. (2016). Maintenance of the Epithelial Barrier and Remodeling of Cell-Cell Junctions during Cytokinesis Article Maintenance of the Epithelial Barrier and Remodeling of Cell-Cell Junctions during Cytokinesis. *Current Biology*, 26. <https://doi.org/10.1016/j.cub.2016.05.036>
- Huber, M., Casares-Arias, J., Fässler, R., Müller, D. J., & Strohmeyer, N. (2023). In mitosis integrins reduce adhesion to extracellular matrix and strengthen adhesion to adjacent cells. *Nature Communications* 2023 14:1, 14(1), 1–17. <https://doi.org/10.1038/s41467-023-37760-x>
- Igaki, T., Pastor-Pareja, J. C., Aonuma, H., Miura, M., & Xu, T. (2009). Intrinsic Tumor Suppression and Epithelial Maintenance by Endocytic Activation of Eiger/TNF Signaling in Drosophila. *Developmental Cell*, 16(3), 458–465. <https://doi.org/10.1016/J.DEVCEL.2009.01.002>
- Ikawa, K., Ishihara, S., Tamori, Y., & Sugimura, K. (2023). Attachment and detachment of cortical myosin regulates cell junction exchange during cell rearrangement in the Drosophila wing epithelium. *Current Biology*: CB, 33(2), 263-275.e4. <https://doi.org/10.1016/J.CUB.2022.11.067>
- Izumi, Y., & Furuse, M. (2014). Molecular organization and function of invertebrate occluding junctions. *Seminars in Cell & Developmental Biology*, 36, 186–193. <https://doi.org/10.1016/J.SEMCDB.2014.09.009>
- Karim, F. D., & Rubin, G. M. (1998). Ectopic expression of activated Ras1 induces hyperplastic growth and increased cell death in Drosophila imaginal tissues. *Development*, 125(1), 1–9. <https://doi.org/10.1242/dev.125.1.1>
- Kyuno, D., Takasawa, A., Kikuchi, S., Takemasa, I., Osanai, M., & Kojima, T. (2021). Role of tight junctions in the epithelial-to-mesenchymal transition of cancer cells. *Biochimica et Biophysica Acta (BBA) - Biomembranes*, 1863(3), 183503. <https://doi.org/10.1016/J.BBAMEM.2020.183503>
- Langhe, R. P., Gudzenko, T., Bachmann, M., Becker, S. F., Gonnermann, C., Winter, C., Abbruzzese, G., Alfandari, D., Kratzer, M. C., Franz, C. M., & Kashef, J. (2016). Cadherin-11 localizes to focal adhesions and promotes cell–substrate adhesion. *Nature Communications* 2016 7:1, 7(1), 1–10. <https://doi.org/10.1038/ncomms10909>
- Levayer, R. (2018). Cell Competition: How to Take Over the Space Left by Your Neighbours. In *Current Biology* (Vol. 28, Issue 13, pp. R741–R744). Cell Press. <https://doi.org/10.1016/j.cub.2018.05.023>
- Levayer, R., Dupont, C., & Moreno, E. (2016). Tissue Crowding Induces Caspase-Dependent Competition for Space. *Current Biology*, 26(5), 670–677. <https://doi.org/10.1016/j.cub.2015.12.072>
- Levayer, R. (2024). Staying away from the breaking point: Probing the limits of epithelial cell elimination. *Current Opinion in Cell Biology*, 86, 102316. <https://doi.org/10.1016/J.CEB.2023.102316>

- Luo, L., & Wu, J. S. (2007). A protocol for mosaic analysis with a repressible cell marker (MARCM) in *Drosophila*. *Nature Protocols* 2006 1:6, 1(6), 2583–2589. <https://doi.org/10.1038/NPROT.2006.320>
- Manninen, A. (2015). Epithelial polarity – Generating and integrating signals from the ECM with integrins. *Experimental Cell Research*, 334(2), 337–349. <https://doi.org/10.1016/J.YEXCR.2015.01.003>
- Manning, L. A., Perez-Vale, K. Z., Schaefer, K. N., Sewell, M. T., & Peifer, M. (2019). The *Drosophila* Afadin and ZO-1 homologues Canoe and Polychaetoid act in parallel to maintain epithelial integrity when challenged by adherens junction remodeling. *Molecular Biology of the Cell*, 30(16), 1938–1960. <https://doi.org/10.1091/MBC.E19-04-0209/ASSET/IMAGES/LARGE/MBE-30-1938-G010.JPEG>
- Mao, Y., Tournier, A. L., Hoppe, A., Kester, L., Thompson, B. J., & Tapon, N. (2013). Differential proliferation rates generate patterns of mechanical tension that orient tissue growth. *The EMBO Journal*, 32(21), 2790. <https://doi.org/10.1038/EMBOJ.2013.197>
- Marinari, E., Mehonic, A., Curran, S., Gale, J., Duke, T., & Baum, B. (2012). Live-cell delamination counterbalances epithelial growth to limit tissue overcrowding. *Nature*, 484(7395), 542–545. <https://doi.org/10.1038/NATURE10984>
- Maurer, P., Laplantine, E., Vallar, L., Eble, J., Paulsson, M., Bruckner, P., Kieffer, N., & Aumailley, M. (2002). The integrin  $\beta 1$  subunit cytoplasmic tail forms oligomers: a potential role in  $\beta 1$  integrin clustering. *Biology of the Cell*, 94(6), 375–387. [https://doi.org/10.1016/S0248-4900\(02\)00009-6](https://doi.org/10.1016/S0248-4900(02)00009-6)
- McMahon, A., Reeves, G. T., Supatto, W., & Stathopoulos, A. (2010). Mesoderm migration in *Drosophila* is a multi-step process requiring FGF signaling and integrin activity. *Development*, 137(13), 2167–2175. <https://doi.org/10.1242/DEV.051573>
- Mehrbod, M., & Mofrad, M. R. K. (2013). Localized Lipid Packing of Transmembrane Domains Impedes Integrin Clustering. *PLOS Computational Biology*, 9(3), e1002948. <https://doi.org/10.1371/JOURNAL.PCBI.1002948>
- Menéndez, J., Pérez-Garijo, A., Calleja, M., & Morata, G. (2010). A tumor-suppressing mechanism in *Drosophila* involving cell competition and the Hippo pathway. *Proceedings of the National Academy of Sciences of the United States of America*, 107(33), 14651–14656. [https://doi.org/10.1073/PNAS.1009376107/SUPPL\\_FILE/PNAS.201009376SI.PDF](https://doi.org/10.1073/PNAS.1009376107/SUPPL_FILE/PNAS.201009376SI.PDF)
- Miles, W. O., Dyson, N. J., & Walker, J. A. (2011). Modeling tumor invasion and metastasis in *Drosophila*. *Disease Models & Mechanisms*, 4(6), 753–761. <https://doi.org/10.1242/DMM.006908>
- Mira-Osuna, M., & Le Borgne, R. (2024). Assembly, dynamics and remodeling of epithelial cell junctions throughout development. *Development (Cambridge)*, 151(1). <https://doi.org/10.1242/DEV.201086/341224>
- Monier, B., Gettings, M., Gay, G., Mangeat, T., Schott, S., Guarner, A., & Suzanne, M. (2015). Apico-basal forces exerted by apoptotic cells drive epithelium folding. *Nature* 2015 518:7538, 518(7538), 245–248. <https://doi.org/10.1038/nature14152>
- Morata, G. (2021). Cell competition: A historical perspective. *Developmental Biology*, 476, 33–40. <https://doi.org/10.1016/J.YDBIO.2021.02.012>
- Morata, G., & Ripoll, P. (1975). Minutes: Mutants of *Drosophila* autonomously affecting cell division rate. *Developmental Biology*, 42(2), 211–221. [https://doi.org/10.1016/0012-1606\(75\)90330-9](https://doi.org/10.1016/0012-1606(75)90330-9)
- Moreno, E., & Basler, K. (2004). dMyc transforms cells into super-competitors. *Cell*, 117(1), 117–129. [https://doi.org/10.1016/S0092-8674\(04\)00262-4](https://doi.org/10.1016/S0092-8674(04)00262-4)
- Moreno, E., Valon, L., Levillayer, F., & Levayer, R. (2019). Competition for Space Induces Cell Elimination through Compaction-Driven ERK Downregulation. *Current Biology*, 29(1), 23. <https://doi.org/10.1016/J.CUB.2018.11.007>
- Narasimha, M., & Brown, N. H. (2004). Novel Functions for Integrins in Epithelial Morphogenesis. *Current Biology*, 14(5), 381–385. <https://doi.org/10.1016/J.CUB.2004.02.033>
- Ohsawa, S., Vaughen, J., & Igaki, T. (2018). Cell Extrusion: A Stress-Responsive Force for Good or Evil in Epithelial Homeostasis. *Developmental Cell*, 44(3), 284–296. <https://doi.org/10.1016/J.DEVCEL.2018.01.009>

- O'Keefe, D. D., Gonzalez-Niño, E., Burnett, M., Dylla, L., Lambeth, S. M., Licon, E., Amesoli, C., Edgar, B. A., & Curtiss, J. (2009). Rap1 maintains adhesion between cells to affect Egfr signaling and planar cell polarity in *Drosophila*. *Developmental Biology*, 333(1), 143–160. <https://doi.org/10.1016/J.YDBIO.2009.06.032>
- Oshima, K., & Fehon, R. G. (2011). Analysis of protein dynamics within the septate junction reveals a highly stable core protein complex that does not include the basolateral polarity protein Discs large. *Journal of Cell Science*, 124(Pt 16), 2861–2871. <https://doi.org/10.1242/JCS.087700>
- Padash-Barmchi, M., Browne, K., Sturgeon, K., Jusiak, B., & Auld, V. J. (2010). Control of Gliotactin localization and levels by tyrosine phosphorylation and endocytosis is necessary for survival of polarized epithelia. *Journal of Cell Science*, 123(23), 4052–4062. <https://doi.org/10.1242/JCS.066605>
- Padash-Barmchi, M., Charish, K., Que, J., & Auld, V. J. (2013). Gliotactin and Discs large are co-regulated to maintain epithelial integrity. *Journal of Cell Science*, 126(Pt 5), 1134–1143. <https://doi.org/10.1242/JCS.113803>
- Pagliarini, R. A., & Xu, T. (2003). A Genetic Screen in *Drosophila* for Metastatic Behavior. *Science*, 302(5648), 1227–1231. <https://doi.org/10.1126/science.1088474>
- Paul, S. M., Ternet, M., Salvaterra, P. M., & Beitel, G. J. (2003). The Na<sup>+</sup>/K<sup>+</sup> ATPase is required for septate junction function and epithelial tube-size control in the *Drosophila* tracheal system. *Development*, 130(20), 4963–4974. <https://doi.org/10.1242/DEV.00691>
- Perdigoto, C. N., Schweisguth, F., & Bardin, A. J. (2011). Distinct levels of Notch activity for commitment and terminal differentiation of stem cells in the adult fly intestine. *Development*, 138(21), 4585–4595. <https://doi.org/10.1242/DEV.065292>
- Pickett, M. A., Naturale, V. F., & Feldman, J. L. (2019). A Polarizing Issue: Diversity in the Mechanisms Underlying Apico-Basolateral Polarization In Vivo. <https://doi.org/10.1146/Annurev-Cellbio-100818-125134>, 35, 285–308. <https://doi.org/10.1146/ANNUREV-CELLBIO-100818-125134>
- Pinal, N., Martín, M., Medina, I., & Morata, G. (2018). Short-term activation of the Jun N-terminal kinase pathway in apoptosis-deficient cells of *Drosophila* induces tumorigenesis. *Nature Communications* 2018 9:1, 9(1), 1–10. <https://doi.org/10.1038/s41467-018-04000-6>
- Plunder, S., Danesin, C., Glise, B., Ferreira, M. A., Merino-Aceituno, S., & Theveneau, E. (2024). Modelling variability and heterogeneity of EMT scenarios highlights nuclear positioning and protrusions as main drivers of extrusion. *Nature Communications* 2024 15:1, 15(1), 1–19. <https://doi.org/10.1038/S41467-024-51372-Z>
- Prior, I. A., Hood, F. E., & Hartley, J. L. (2020). The frequency of ras mutations in cancer. *Cancer Research*, 80(14), 2669–2974. <https://doi.org/10.1158/0008-5472.CAN-19-3682/653980/AM/THE-FREQUENCY-OF-RAS-MUTATIONS-IN-CANCER-RAS-CANCER>
- Raab, M., Gentili, M., De Belly, H., Thiam, H. R., Vargas, P., Jimenez, A. J., Lautenschlaeger, F., Voituriez, R., Lennon-Duménil, A. M., Manel, N., & Piel, M. (2016). ESCRT III repairs nuclear envelope ruptures during cell migration to limit DNA damage and cell death. *Science*, 352(6283), 359–362. [https://doi.org/10.1126/SCIENCE.AAD7611/SUPPL\\_FILE/PAPV3.PDF](https://doi.org/10.1126/SCIENCE.AAD7611/SUPPL_FILE/PAPV3.PDF)
- Ready, D. F., Hanson, T. E., & Benzer, S. (1976). Development of the *Drosophila* retina, a neurocrystalline lattice. *Developmental Biology*, 53(2), 217–240. [https://doi.org/10.1016/0012-1606\(76\)90225-6](https://doi.org/10.1016/0012-1606(76)90225-6)
- Robinow, S., & White, K. (1991). Characterization and spatial distribution of the ELAV protein during *Drosophila melanogaster* development. *Journal of Neurobiology*, 22(5), 443–461. <https://doi.org/10.1002/NEU.480220503>
- Rosenblatt, J., Raff, M. C., & Cramer, L. P. (2001). An epithelial cell destined for apoptosis signals its neighbors to extrude it by an actin- and myosin-dependent mechanism. *Current Biology*, 11(23), 1847–1857. [https://doi.org/10.1016/S0960-9822\(01\)00587-5](https://doi.org/10.1016/S0960-9822(01)00587-5)
- Sawyer, J. K., Harris, N. J., Slep, K. C., Gaul, U., & Peifer, M. (2009). The *Drosophila* afadin homologue Canoe regulates linkage of the actin cytoskeleton to adherens junctions during apical constriction. *Journal of Cell Biology*, 186(1), 57–73. <https://doi.org/10.1083/JCB.200904001/VIDEO-6>

- Schindelin, J., Arganda-Carreras, I., Frise, E., Kaynig, V., Longair, M., Pietzsch, T., Preibisch, S., Rueden, C., Saalfeld, S., Schmid, B., Tinevez, J. Y., White, D. J., Hartenstein, V., Eliceiri, K., Tomancak, P., & Cardona, A. (2012). Fiji: An open-source platform for biological-image analysis. *Nature Methods*, *9*(7), 676–682. <https://doi.org/10.1038/NMETH.2019>
- Schulte, J., Tepass, U., & Auld, V. J. (2003). Gliotactin, a novel marker of tricellular junctions, is necessary for septate junction development in *Drosophila*. *Journal of Cell Biology*, *161*(5), 991–1000. <https://doi.org/10.1083/JCB.200303192>
- Sidor, C., & Röper, K. (2017). Squeezing out in a “tug of war”: The role of myosin in neural stem cell delamination. *The Journal of Cell Biology*, *216*(5), 1215. <https://doi.org/10.1083/JCB.201702116>
- Simões, S., Oh, Y., Wang, M. F. Z., Fernandez-Gonzalez, R., & Tepass, U. (2017). Myosin II promotes the anisotropic loss of the apical domain during *Drosophila* neuroblast ingression. *Journal of Cell Biology*, *216*(5), 1387–1404. <https://doi.org/10.1083/JCB.201608038/VIDEO-5>
- Simon, M. A., Bowtell, D. D. L., Dodson, G. S., Laverty, T. R., & Rubin, G. M. (1991). Ras1 and a putative guanine nucleotide exchange factor perform crucial steps in signaling by the sevenless protein tyrosine kinase. *Cell*, *67*(4), 701–716. [https://doi.org/10.1016/0092-8674\(91\)90065-7](https://doi.org/10.1016/0092-8674(91)90065-7)
- Slattum, G., McGee, K. M., & Rosenblatt, J. (2009). P115 RhoGEF and microtubules decide the direction apoptotic cells extrude from an epithelium. *The Journal of Cell Biology*, *186*(5), 693–702. <https://doi.org/10.1083/JCB.200903079>
- Tamori, Y., Suzuki, E., & Deng, W. M. (2016). Epithelial Tumors Originate in Tumor Hotspots, a Tissue-Intrinsic Microenvironment. *PLoS Biology*, *14*(9), e1002537. <https://doi.org/10.1371/JOURNAL.PBIO.1002537>
- Teng, X., Qin, L., Le Borgne, R., & Toyama, Y. (2017). Remodeling of adhesion and modulation of mechanical tensile forces during apoptosis in *Drosophila* epithelium. *Development (Cambridge)*, *144*(1), 95–105. <https://doi.org/10.1242/DEV.139865/VIDEO-16>
- Tepass, U. (2012). The Apical Polarity Protein Network in *Drosophila* Epithelial Cells: Regulation of Polarity, Junctions, Morphogenesis, Cell Growth, and Survival. <https://doi.org/10.1146/Annurev-Cellbio-092910-154033>, *28*, 655–685. <https://doi.org/10.1146/ANNUREV-CELLBIO-092910-154033>
- Tozluoglu, M., & Mao, Y. (2020). On folding morphogenesis, a mechanical problem. *Philosophical Transactions of the Royal Society of London. Series B, Biological Sciences*, *375*(1809). <https://doi.org/10.1098/RSTB.2019.0564>
- Vale, K. Z. P., Yow, K. D., Gurley, N. J., Greene, M., & Peifer, M. (2023). Rap1 regulates apical contractility to allow embryonic morphogenesis without tissue disruption and acts in part via Canoe-independent mechanisms. *Molecular Biology of the Cell*, *34*(1). <https://doi.org/10.1091/MBE.E22-05-0176/ASSET/IMAGES/LARGE/MBC-34-AR7-G011.JPEG>
- Valencia-Expósito, A., Khalilgharibi, N., Mao, Y., & Martín-Bermudo, M. D. (n.d.). *Local weakening of cell-ECM adhesion triggers basal tissue folding via changes in cell shape, actomyosin organization and E-cad levels*. <https://doi.org/10.1101/2024.08.27.609853>
- Vasquez, C. G., De la Serna, E. L., & Dunn, A. R. (2021). How cells tell up from down and stick together to construct multicellular tissues - interplay between apicobasal polarity and cell-cell adhesion. *Journal of Cell Science*, *134*(21). <https://doi.org/10.1242/JCS.248757/272658>
- Ventura, G., Amiri, A., Thiagarajan, R., Tolonen, M., Doostmohammadi, A., & Sedzinski, J. (2022). Multiciliated cells use filopodia to probe tissue mechanics during epithelial integration in vivo. *Nature Communications* *2022 13:1*, *13*(1), 1–15. <https://doi.org/10.1038/s41467-022-34165-0>
- Vidal, M., & Cagan, R. L. (2006). *Drosophila* models for cancer research. *Current Opinion in Genetics & Development*, *16*(1), 10–16. <https://doi.org/10.1016/J.GDE.2005.12.004>
- Villars, A., & Levayer, R. (2022). Collective effects in epithelial cell death and cell extrusion. *Current Opinion in Genetics & Development*, *72*, 8–14. <https://doi.org/10.1016/J.GDE.2021.09.004>
- Villars, A., Matamoro-Vidal, A., Levillayer, F., & Levayer, R. (2022). Microtubule disassembly by caspases is an important rate-limiting step of cell extrusion. *Nature Communications* *2022 13:1*, *13*(1), 1–18. <https://doi.org/10.1038/s41467-022-31266-8>

- Walther, R. F., Burki, M., Pinal, N., Rogerson, C., & Pichaud, F. (2018). Rap1, Canoe and Mbt cooperate with Bazooka to promote zonula adherens assembly in the fly photoreceptor. *Journal of Cell Science*, 131(6). <https://doi.org/10.1242/JCS.207779/265423/AM/RAP1-CANOE-AND-MBT-COOPERATE-WITH-BAZOOKA-TO>
- Wang, Z., Bosveld, F., & Bellaïche, Y. (2018). Tricellular junction proteins promote disentanglement of daughter and neighbour cells during epithelial cytokinesis. *Journal of Cell Science*, 131(11). <https://doi.org/10.1242/JCS.215764/VIDEO-4>
- Ward, R. E., Schweizer, L., Lamb, R. S., & Fehon, R. G. (2001). The protein 4.1, ezrin, radixin, moesin (FERM) domain of *Drosophila* Coracle, a cytoplasmic component of the septate junction, provides functions essential for embryonic development and imaginal cell proliferation. *Genetics*, 159(1), 219. <https://doi.org/10.1093/GENETICS/159.1.219>
- Warren, J., & Kumar, J. P. (2023). Patterning of the *Drosophila* retina by the morphogenetic furrow. *Frontiers in Cell and Developmental Biology*, 11, 1151348. <https://doi.org/10.3389/FCELL.2023.1151348/BIBTEX>
- Wodarz, A., Ramrath, A., Grimm, A., & Knust, E. (2000). *Drosophila* Atypical Protein Kinase C Associates with Bazooka and Controls Polarity of Epithelia and Neuroblasts. *The Journal of Cell Biology*, 150(6), 1361. <https://doi.org/10.1083/JCB.150.6.1361>
- Wolff, T., & Ready, D. F. (1991). The beginning of pattern formation in the *Drosophila* compound eye: the morphogenetic furrow and the second mitotic wave. *Development*, 113(3), 841–850. <https://doi.org/10.1242/DEV.113.3.841>
- Wu, M., Pastor-Pareja, J. C., & Xu, T. (2010). Interaction between RasV12 and scribbled clones induces tumour growth and invasion. *Nature*, 463(7280), 545–548. <https://doi.org/10.1038/nature08702>
- Yang, L., & Baker, N. E. (2003). Cell Cycle Withdrawal, Progression, and Cell Survival Regulation by EGFR and Its Effectors in the Differentiating *Drosophila* Eye. *Developmental Cell*, 4(3), 359–369. [https://doi.org/10.1016/S1534-5807\(03\)00059-5](https://doi.org/10.1016/S1534-5807(03)00059-5)
- Yang, J., Antin, P., Berx, G., Blanpain, C., Brabletz, T., Bronner, M., Campbell, K., Cano, A., Casanova, J., Christofori, G., Dedhar, S., Derynck, R., Ford, H. L., Fuxe, J., García de Herreros, A., Goodall, G. J., Hadjantonakis, A. K., Huang, R. J. Y., Kalcheim, C., ... Sheng, G. (2020). Guidelines and definitions for research on epithelial-mesenchymal transition. *Nature Reviews. Molecular Cell Biology*, 21(6), 341–352. <https://doi.org/10.1038/S41580-020-0237-9>
- Yost, P. P., Al-Nouman, A., & Curtiss, J. (2023). The Rap1 small GTPase affects cell fate or survival and morphogenetic patterning during *Drosophila melanogaster* eye development. *Differentiation*, 133, 12–24. <https://doi.org/10.1016/J.DIFF.2023.06.001>
- Yu, H. H., & Zallen, J. A. (2020). Abl and Canoe/Afadin mediate mechanotransduction at tricellular junctions. *Science (New York, N.Y.)*, 370(6520). <https://doi.org/10.1126/SCIENCE.ABA5528>
- Zappia, M. P., Brocco, M. A., Billi, S. C., Frasnich, A. C., & Ceriani, M. F. (2011). M6 Membrane Protein Plays an Essential Role in *Drosophila* Oogenesis. *PLoS ONE*, 6(5), 19715. <https://doi.org/10.1371/journal.pone.0019715>

## Figure and Figure legends

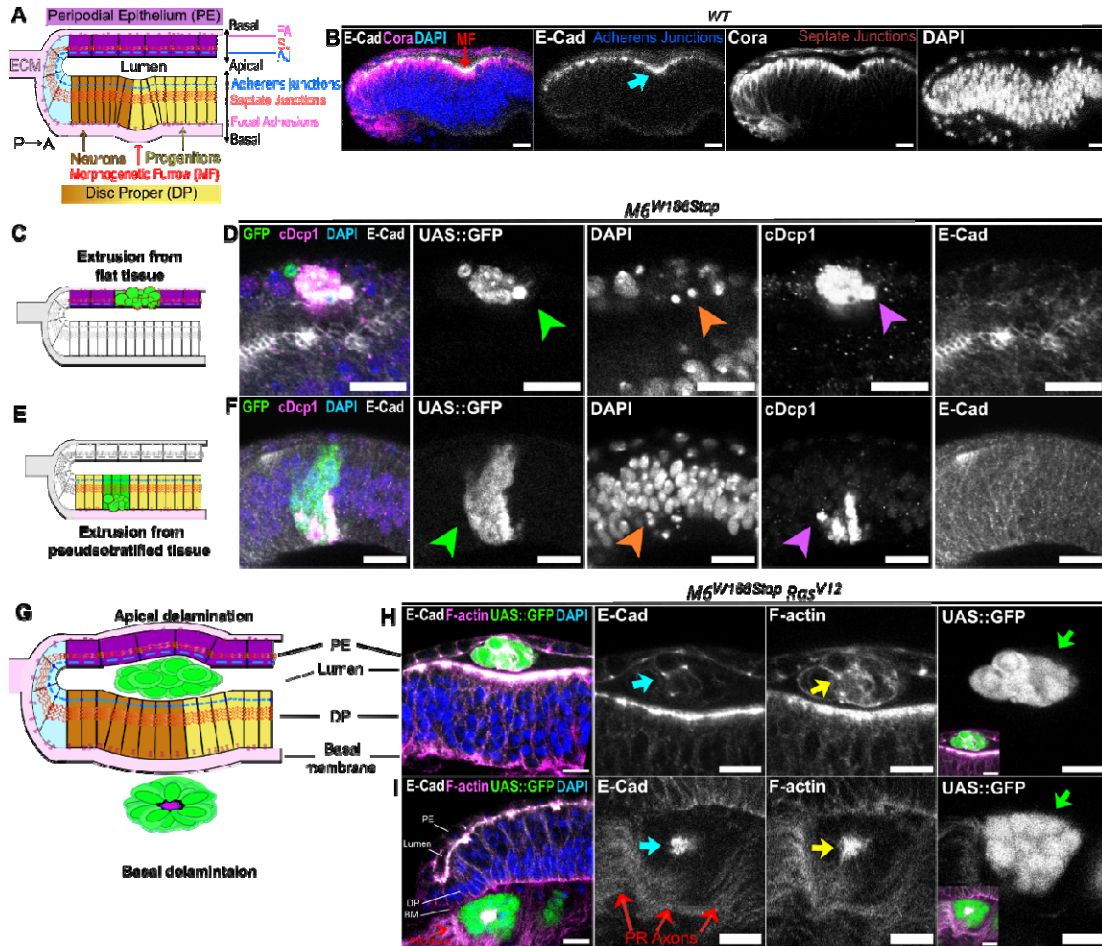


### Figure 1. Loss of septate junction integrity in tumors triggers collective delamination of living cells from the *Drosophila* eye disc

(A, C, E, G) Schematic of an orthogonal section along the dorso-ventral axis of the *Drosophila* eye disc (A), apical and basal extrusion (C, E) and apical and basal delamination (G). In this and the following panels, the anterior-posterior axis is left-to-right, the peripodial epithelium (PE) in violet, undifferentiated cells in the Disc Proper (DP) in yellow, differentiated cells in the PD in brown, adherens junctions (AJ) in blue, septate junctions (SJ) in red, focal adhesions (FA) in magenta, the extracellular matrix (ECM) in light pink. Green cells show clones generated with the eyMARCM system.

(B) Wild-type eye disc immunostained for E-cad, main component of adherens junctions, Coracle, core-complex SJ component, and DAPI. During development, the eye disc undergoes neurogenesis and the forefront of the antero-posterior wave of differentiation is termed the morphogenetic furrow (MF, red arrow). MF is observed by the transient apical constriction of cells in the pseudostratified epithelium (blue arrow) and can be used as a topological landmark.

(D, F) Homozygous mutant clones for M6 (*M6<sup>W186Stop</sup>*, green) undergo extrusion in the flat (D) and in the pseudostratified (F) epithelium. Mutant clones (green arrowheads) contain

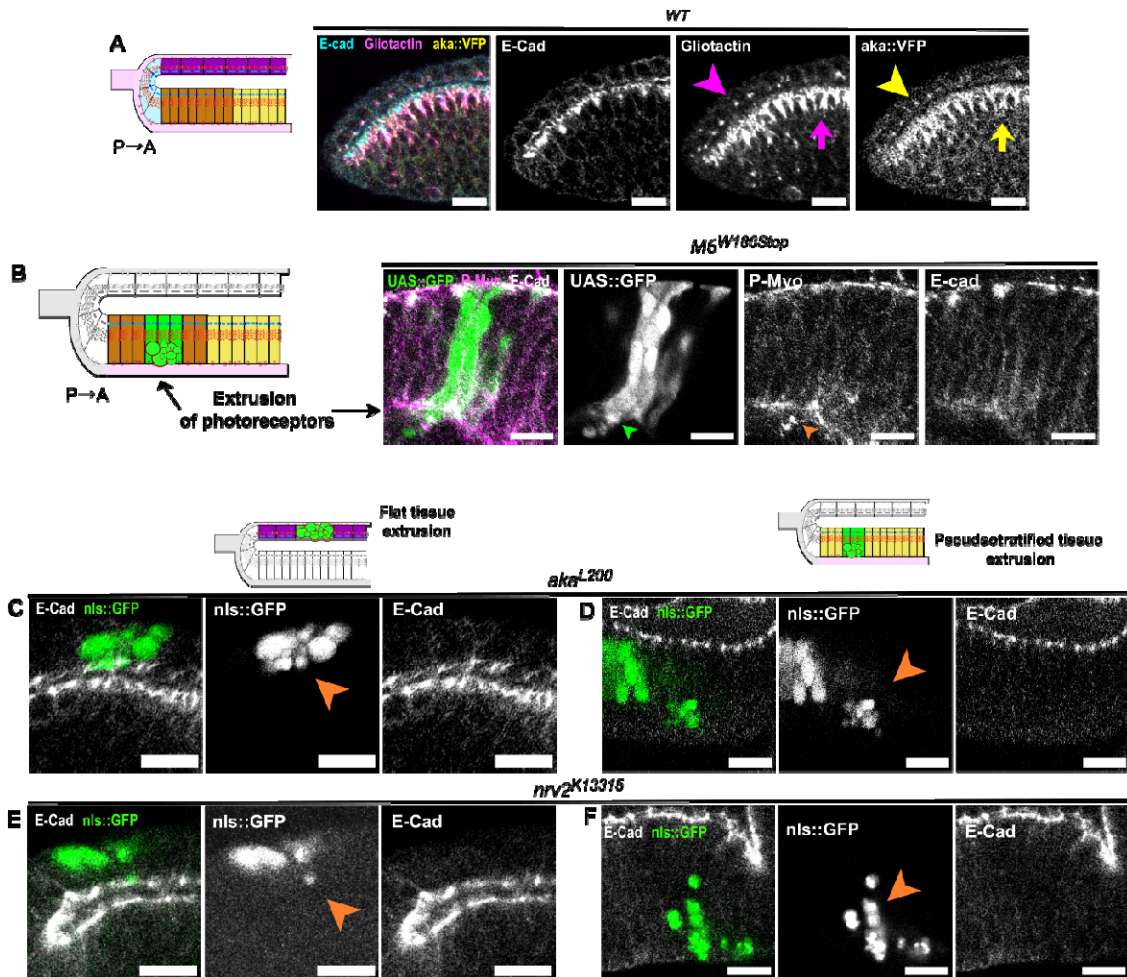


pyknotic nuclei (orange arrowheads) and are positive for the *Drosophila* caspase-1 (DCP-1) antibody (violet arrowheads), an upstream activator of the caspase cascade.

(H, I) Homozygous mutant clones for M6 and overactivated Ras ( $M6^{W186Stop} Ras^{V12}$ , green) collectively delaminate apically in the lumen (H) and basal to the eye disc (I). Apical and basal delaminated cells are organized in clusters (green arrows), yet depending on the directionality of delamination, junctional (E-cad, blue arrow) and activated actomyosin cytoskeleton regulators markers (F-actin, yellow arrow) have striking different localization. (H) Mutant cells having undergone apical collective delamination appear in the lumen with E-cad and F-actin localized along the cell membranes. (I) Mutant cells having undergone basal collective delamination formed radial structures termed rosettes in which E-cad and F-actin localization is restricted to the central domain. Photoreceptor axons (PR axons, red arrows) can be observed in the most posterior part of the disc.

The scale bars represent 10  $\mu\text{m}$ . All images are single confocal optical sections with posterior to the left, anterior to the right. See also Figure S1.

Figure S1. Microscopy images, related to Figures 1



### Supplementary Figure 1. Microscopy images, related to Figures 1 Septate junction loss triggers extrusion in the eye disc

(A, B) Schematic of an orthogonal section along the dorso-ventral axis of the *Drosophila* eye and confocal microscopy images of eye-antennal larval imaginal discs.

(A) wild-type eye disc immunostained for E-cad (grey) and Gli (magenta) where all cells express the endogenously tagged aka::VFP (yellow). Cells in the flat epithelium express Gli

and aka (pink and yellow arrowheads, respectively), as well as cells in the pseudostratified epithelium (pink and yellow arrows, respectively).

(B) Heterozygous eye disc comprised of wild-type and mutant clones tagged with GFP and defective for the tricellular SJ master regulator M6 ( $M6^{W186Stop}$ , green). Mutant cells (green arrowhead) in the differentiated part of the eye disc, posterior to the MF, where photoreceptors and interommatidial cells are found, contain fragmented cytoplasm (green arrowhead) strongly stained with P-Myo (orange arrowhead), a hallmark of apoptotic bodies and cell extrusion.

(C, D) Heterozygous eye disc comprised of wild-type and mutant clones tagged with GFP and defective for the tricellular SJ master regulator Aka ( $aka^{L200}$ , green). Mutant cells in the peripodial epithelium (C) and in the pseudostratified epithelium (D) contain pyknotic bodies, suggesting they are eliminated from the tissue via caspase-activated cell extrusion (orange arrowheads).

(E, F) Heterozygous eye disc comprised of wild-type and mutant clones tagged with GFP and defective for the bicellular SJ core-complex component Nrv2 ( $Nrv2^{K3315}$ , green). Mutant cells in the peripodial epithelium (E) and in the pseudostratified epithelium (F) pyknotic bodies, suggesting they are eliminated from the tissue via caspase-activated cell extrusion (orange arrowheads).

The scale bars represent 10  $\mu\text{m}$ . All images are single confocal optical sections with posterior to the left, anterior to the right. See also Figure 1.

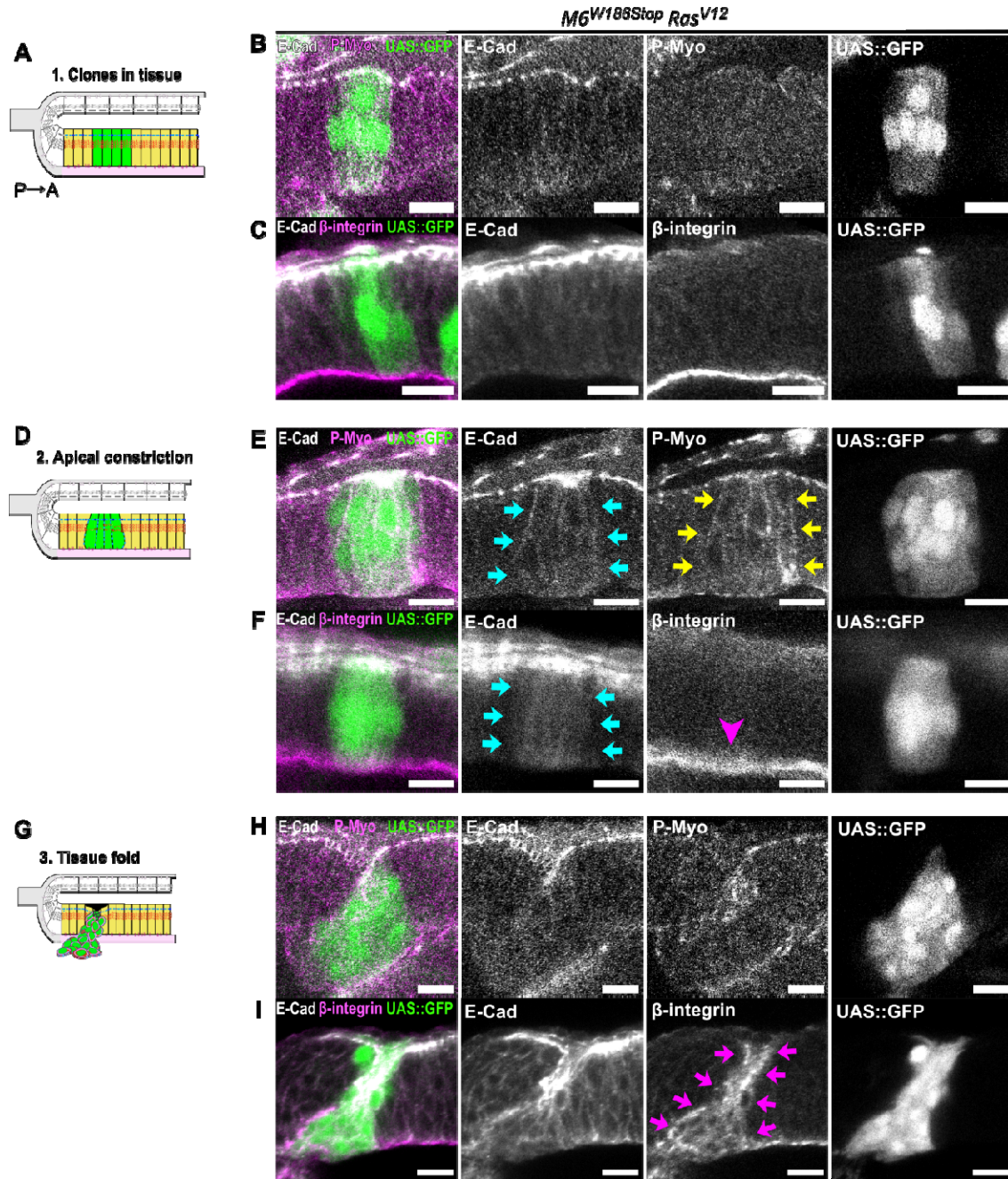


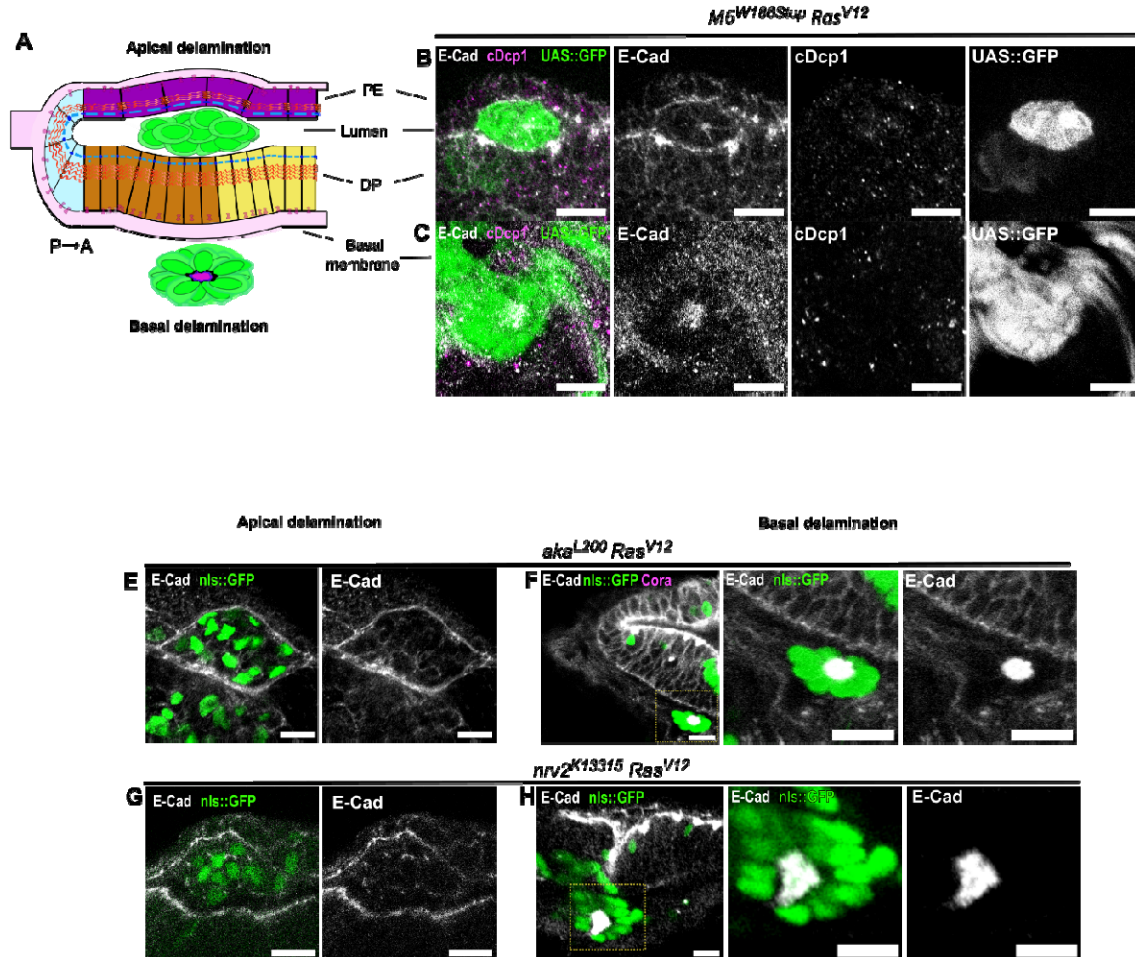
**Figure 2. Mutant cells expressing oncogenic Ras form tissue fold anterior to the MF after apical constriction and basolateral delocalization of E-cadherin**

(A, D, G) Schematic of an orthogonal section along the dorso-ventral axis of the *Drosophila* eye disc in the undifferentiated region of the pseudostratified epithelium (yellow). Mutant cells (green) initially showcase no difference to their wild-type counterparts (A), then become apically constricted (D) and finally form tissue folds (G).

(B, C, E, F, H, I) Heterozygous eye disc immunostained with anti-E-cad (grey) and anti-P-Myo (B, E, H, magenta) or anti-β-integrin (C, F, I, magenta). Homozygous mutant cells for M6 (*M6<sup>W186Stop</sup>*) and oncogenic Ras cells express the clone marker UAS::GFP (green).

(B, C) Mutant cells anterior to the MF showcase no differences in terms adherens junctions, focal adhesions or cytoskeleton remodeling. (E, F) Apical constriction of mutant cells is concomitant with E-cad basolateral spreading (blue arrows) and basolateral cytoskeleton

remodeling (green arrows), while  $\beta$ -integrin -mediated anchoring to the extracellular matrix is preserved (pink arrowhead). (H, I) Lastly, mutant cells continue to apically constrict their surface and invaginate and exhibit basolateral spreading of E-cad and activated cytoskeleton regulators, together with basolateral spreading of  $\beta$ -integrin (pink arrows). The scale bars represent 10  $\mu$ m. All images are single confocal optical sections with posterior to the left, anterior to the right. See also Figure S2.



### Supplementary Figure 2. Microscopy images, related to Figures 2 Septate junction loss in synergy with Ras transformation triggers collective delamination in the eye disc

(A) Schematic of an orthogonal section along the dorso-ventral axis of the *Drosophila* eye antennal larval imaginal discs where SJ-deficient RasV12 mutant cells undergo apical and basal collective delamination.

(B, C) Heterozygous eye discs immunostained with anti-E-cad (grey) and anti-Drosophila caspase-1 (DCP-1) (C, magenta). Clones tagged with GFP are mutant for M6 and express overactivated Ras ( $M6^{W186Stop} Ras^{V12}$ , green). Mutant cells delaminate collectively and alive out of an epithelium, either apically, appearing in the lumen (B), or basally, forming rosettes basal to the eye disc (C).

(E, F) Heterozygous eye discs immunostained with anti-E-cad (grey). Clones tagged with GFP are mutant for aka and express overactivated Ras ( $aka^{L200P} Ras^{V12}$ , green). Mutant cells

delaminate collectively and alive out of an epithelium, either apically, appearing in the lumen (E), or basally, forming rosettes basal to the eye disc (F).

(G, H) Heterozygous eye discs immunostained with anti-E-cad (grey). Clones tagged with GFP are mutant for Nrv2 and express overactivated Ras ( $nrv2^{K13315} Ras^{V12}$ , green). Mutant cells delaminate collectively and alive out of an epithelium, either apically, appearing in the lumen (G), or basally, forming rosettes basal to the eye disc (H).

The scale bars represent 10  $\mu\text{m}$ . All images are single confocal optical sections with posterior to the left, anterior to the right. See also Figure 2.

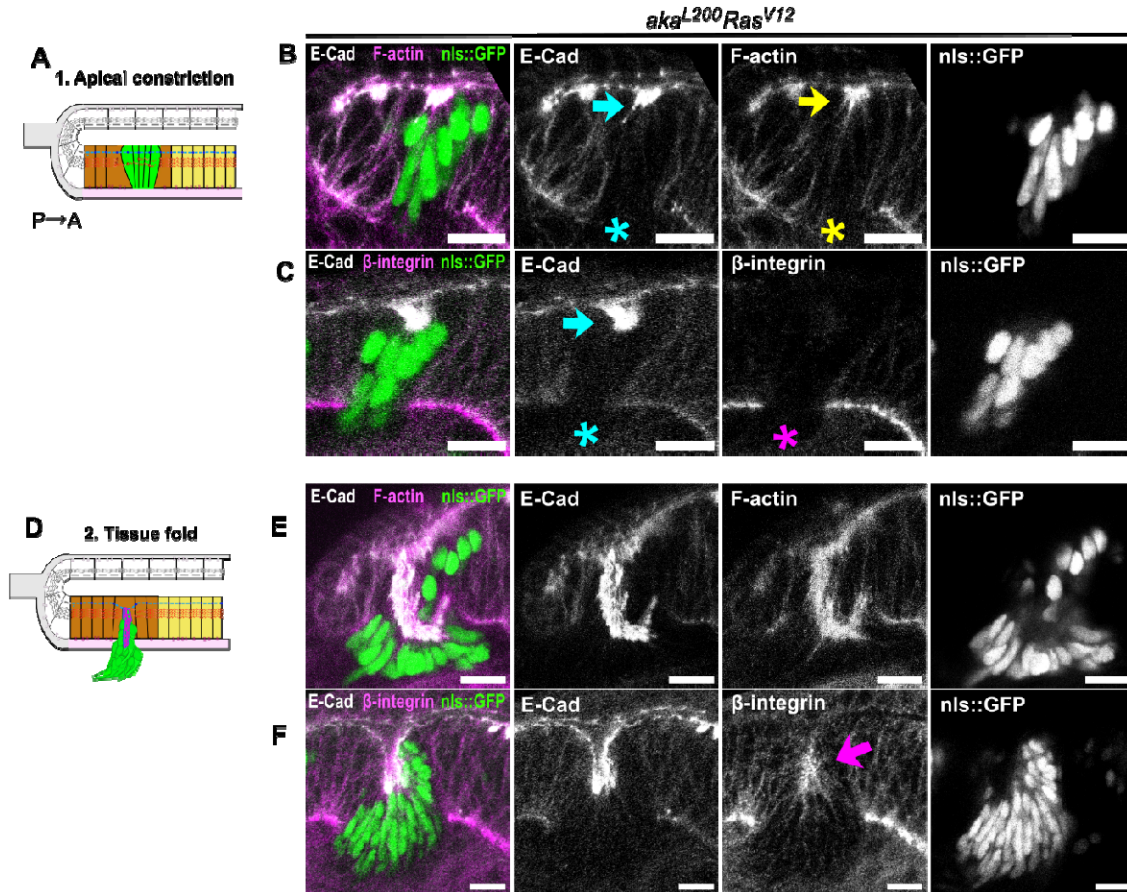


**Figure 3. Mutant cells expressing oncogenic Ras form tissue fold anterior to the MF after apical constriction and basolateral delocalization of E-cadherin**

(A, D) Schematic of an orthogonal section along the dorso-ventral axis of the *Drosophila* eye disc in the differentiated region of the pseudostratified epithelium (brown), anterior to undifferentiated cells (yellow). Mutant cells (green) apically constrict (A) to then form tissue folds (D).

(B, C, E, F) Heterozygous eye disc immunostained with anti-E-cad (grey) and phalloidin (B, E, H magenta) or anti- $\beta$ -integrin (C, F, magenta). Homozygous mutant cells for *aka* ( $aka^{L200}$ ) and oncogenic Ras cells express the clone marker nls::GFP (green).

(B, C) At xx h AEL, mutant cells posterior to the MF appear apically constricted (blue arrows) and have lost the basal loss of E-cad (blue asterisk). Anchoring to the extracellular matrix is lost, as observed by the basal loss of  $\beta$ -integrin (pink asterisk) and actin stress fibers (yellow asterisk). (E, F) Mutant cells continue to exhibit apical constriction and invaginate. Apical enrichment of  $\beta$ -integrin (pink arrow) is observed, suggested preferential adhesion between mutant cells is present.

The scale bars represent 10  $\mu\text{m}$ . All images are single confocal optical sections with posterior to the left, anterior to the right. See also Figure S3.

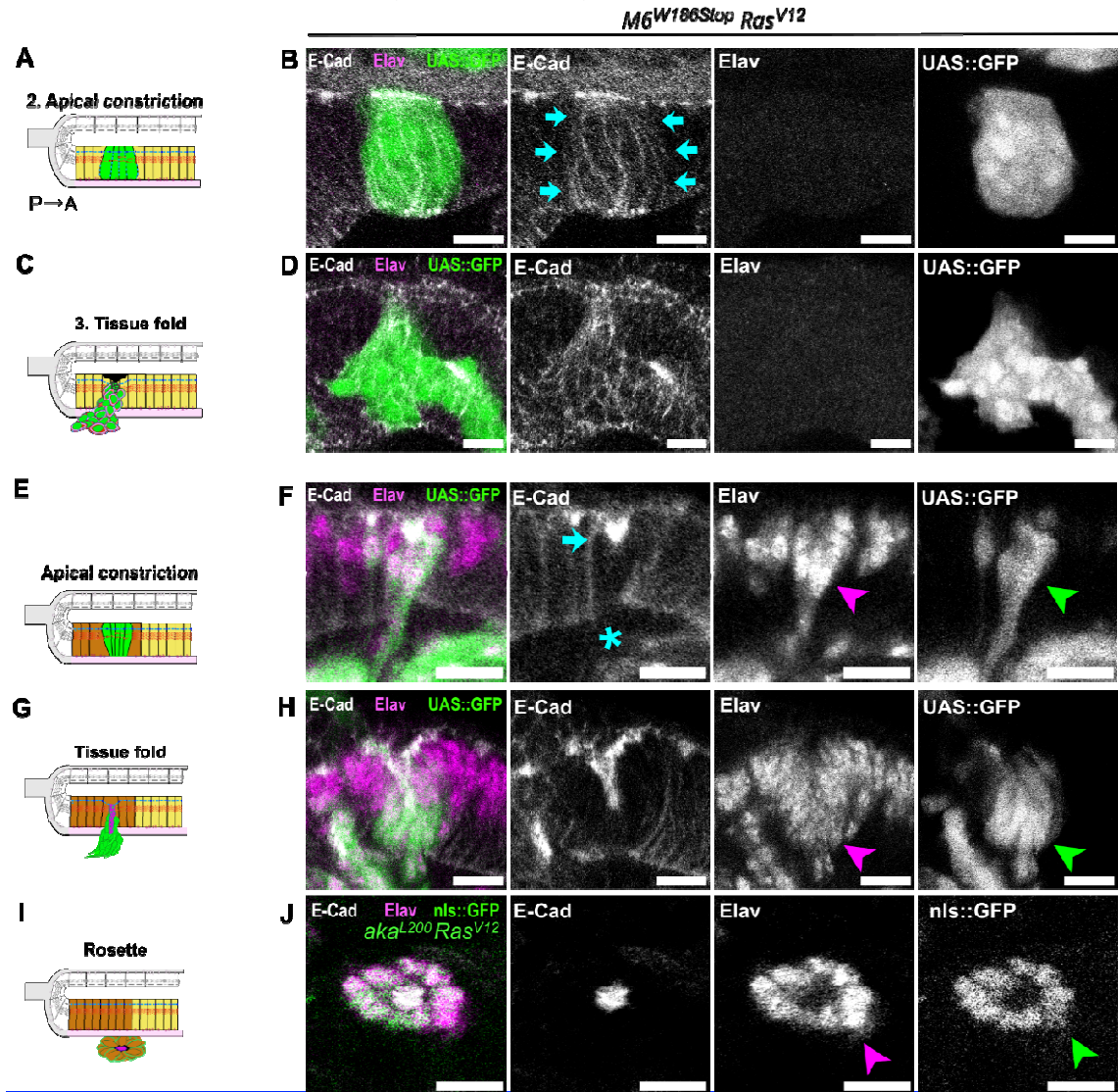


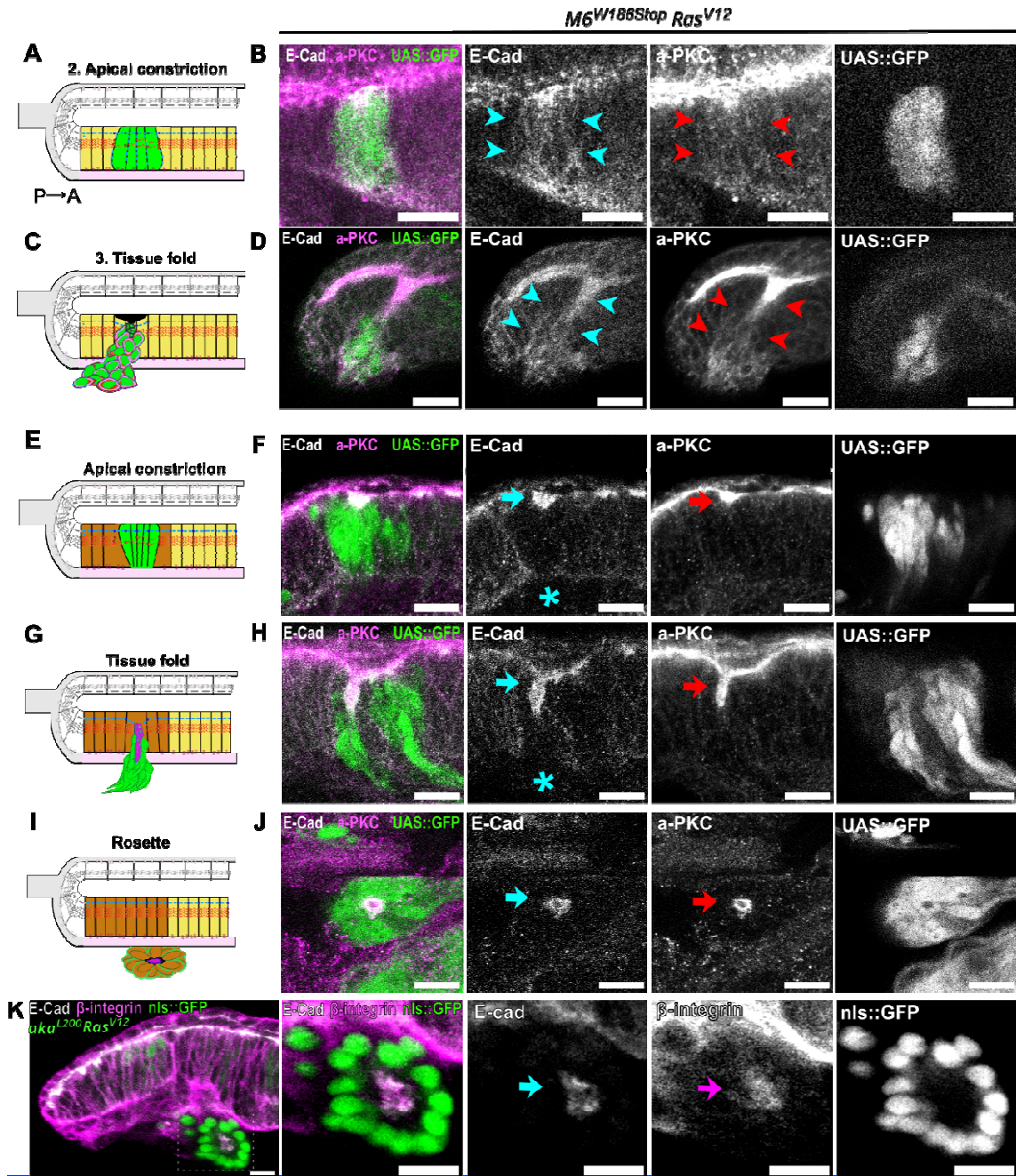
**Figure 4. Rosettes are exclusively formed by polarized differentiated cells while tissue folds arise from either undifferentiated unpolarized cells, or differentiated polarized cells**

(A, C, E, G, I) Schematic of an orthogonal section along the dorso-ventral axis of the *Drosophila* eye disc of collective multicellular rearrangements with basal directionality that arise from the pseudostratified epithelium (brown, yellow).

(B, C, E, F) Heterozygous eye disc immunostained with and stained with anti-*E-cad* (grey) and anti-Elav (pan-neuronal cell marker, magenta). Homozygous mutant cells for M6 (*M6<sup>W186Stop</sup>*) and oncogenic Ras cells express the clone marker UAS::GFP (green). (B) Clones in the undifferentiated region of the pseudostratified epithelium anterior to the MF, when they undergo apical constriction with basolateral spreading of E-cad (blue arrow), are formed by clusters of xx cells, homogenously negative for Elav. (D) Tissue folds formed anterior to the MF are also homogenously negative for Elav. (F) Clones in the differentiated region of the pseudostratified epithelium (green arrowhead), posterior to the MF, are homogenously positive for Elav (magenta arrow head) when they initially undergo apical constrict (blue arrow) and loss of basal adhesion to the extracellular matrix (blue asterisk). (F) Tissue folds formed posterior to the MF (green arrowhead) are formed by homogenously

Elav-positive cells (magenta arrowhead). Rosettes are exclusively formed by Elav-expressing cells (magenta arrowheads, green arrowhead). The scale bars represent 10  $\mu\text{m}$ . All images are single confocal optical sections with posterior to the left, anterior to the right. See also Figure S3.

**Figure S3. Microscopy images, related to Figures 3 and 4**



**Supplementary Figure 3. Microscopy images, related to Figures 4. Rosettes are formed independently of tissue folds.**

(A, C, E, G, I) Schematic of an orthogonal section along the dorso-ventral axis of the *Drosophila* eye antennal larval imaginal discs where SJ-deficient RasV12 mutant cells

undergo tissue folding anterior (A, C, yellow) or posterior (E, G, brown) to the MF. Rosettes are formed by differentiated cells (I, brown).

(B, D, F, H, J) Heterozygous eye discs immunostained with anti-E-cad (grey) and anti-aPKC (aPKC, magenta). Clones tagged with GFP are mutant for M6 and express overactivated Ras ( $M6^{W186Stop} Ras^{V12}$ , green).

(B, D) Mutant cells anterior to the MF apically constrict (B) and form tissue folds (D). During both events, basolateral E-cad delocalization (blue arrowheads) is concomitant with a partial loss of polarity, noted by the partial basal localization of aPKC not seen in the wild-type cells (red arrowheads).

(F, H) Mutant cells posterior to the MF apically constrict (F) and form tissue folds (H). During both events, E-cad appear well localized apically (blue arrow) and the basal pool of E-cad is lost (blue asterisk). During both events cell polarity is preserved, as noted by the apical restriction of aPKC (red arrows).

(J) Rosettes are formed by a polarized cluster of cells organized radially that exhibit Ecad at the center (blue arrow), corresponds to the apical domain, as noted by aPKC restricted (red arrow).

(K) Heterozygous eye discs immunostained with anti-E-cad (grey) and anti- $\beta$ -integrin (magenta). Clones tagged with GFP are mutant for aka and express overactivated Ras ( $aka^{L200} Ras^{V12}$ , green) Rosettes exhibit adhesion proteins at the center of the radial cluster, at the apical domain, namely E-cad (blue arrow) and  $\beta$ -integrin (pink arrow).

The scale bars represent 10  $\mu\text{m}$ . All images are single confocal optical sections with posterior to the left, anterior to the right. See also Figure 4.



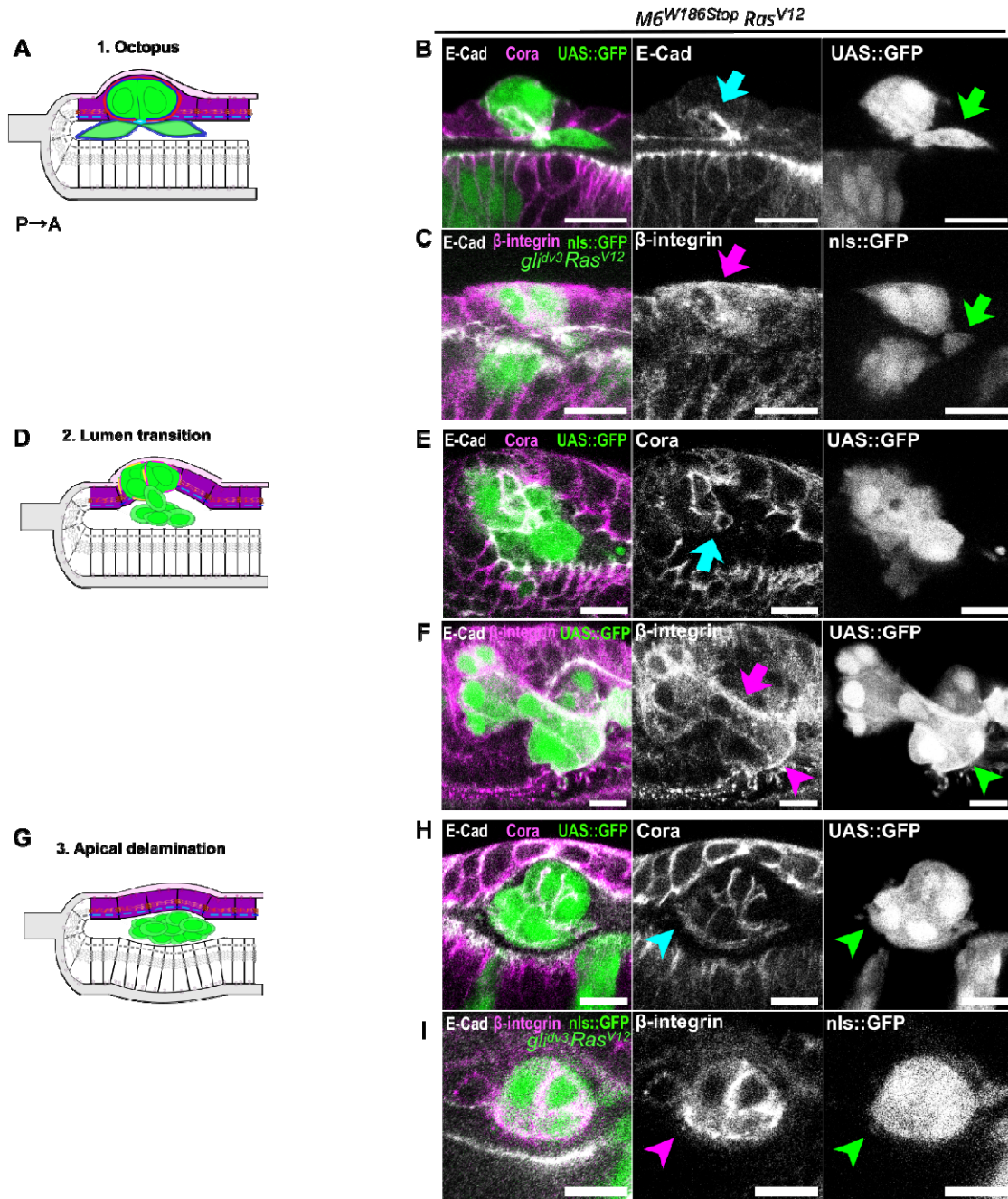


**Figure 5 Apical Delamination of mutant cells from the flat epithelium form an octopus and an apical neck before translocating in the lumen**

(A, D, G) Schematic of an orthogonal section along the dorso-ventral axis of the *Drosophila* eye disc of the flat epithelium (purple). Mutant cells (green) apically constrict (A), progressively translocate into the lumen (D) and ultimately appear completely detached in the lumen (G).

(B, C, E, F, H, I) Heterozygous eye disc immunostained with anti-E-cad (grey) and anti-Cora (B, E, H, magenta) or anti-β-integrin (C, F, I, magenta). Homozygous mutant cells for M6 (*M6<sup>W186Stop</sup>*) and oncogenic Ras cells express the clone marker UAS::GFP (green).

(B, C) During the time window 89-99hAEL, mutant cells in the flat epithelium (green) appear apically constricted and acquire a dome-shape, termed the octopus, which exhibits basolateral enrichment of E-cad (green arrow) and β-integrin (magenta arrow), and apical

lumen protrusions (green arrow). (E, F) Between 90-115hAEL, mutant cells progressively translocate into the lumen (green arrowhead) through a ring-like structure enriched in Cora (blue arrow).  $\beta$ -integrin enrichment is present all throughout the clone, in cells moving from the flat epithelium into the lumen (pink arrow) and cells located in the lumen (pink arrowhead) as (H, I) Lastly, between 114-120hAEL, mutant cells (green) appear completely detached in the lumen, with no connection to the flat epithelium (blue arrowhead) and enriched in  $\beta$ -integrin (pink arrowhead). The scale bars represent 10  $\mu$ m. All images are single confocal optical sections with posterior to the left, anterior to the right.

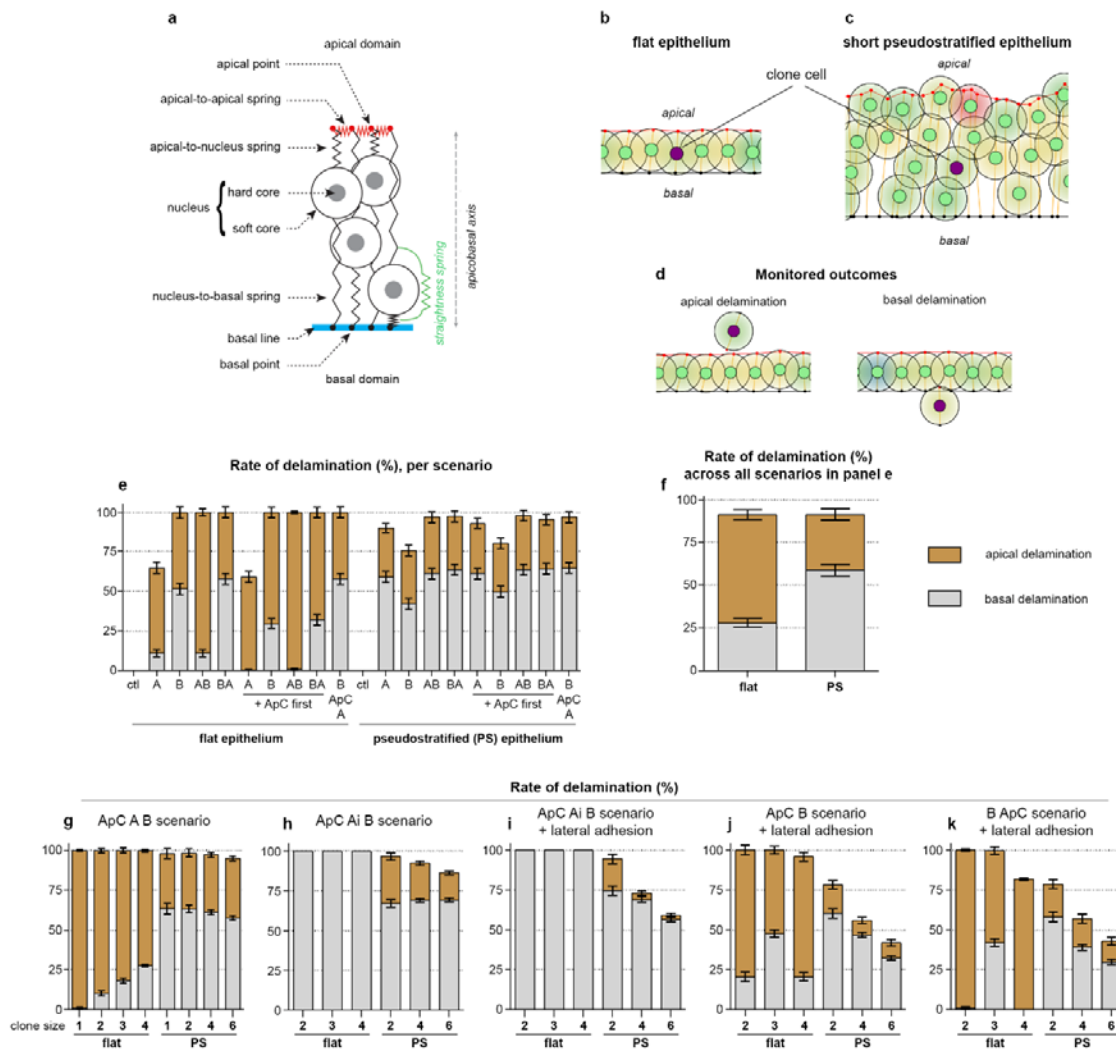
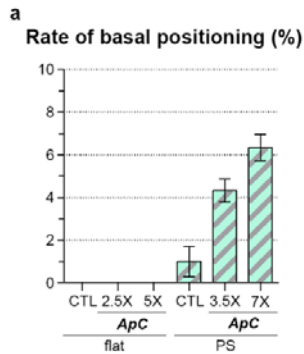


**Figure 6. Differential sensitivity of flat and pseudostratified tissues to simulated epithelial destabilization.**

(A) Diagram representing the simulated cells and the various adjustable springs control their viscoelastic properties. (B, C) Examples of modelling outputs showing the epithelium in flat or short pseudostratified configuration. Control cells have green nuclei, clone cells have magenta nuclei. (D) Examples of apical and basal delamination upon epithelia destabilization. (E) Mean rates of delamination with standard error of the mean for each tested scenario in single cells. (F) Global rate of delamination for all simulations shown in panel E. (G-K) Mean rates of delamination with standard error of the mean for all indicated scenarios tested in clones of various sizes. Each simulation was performed 200 times. A,

loss of apical adhesion between clone cells and between clone cells and control cells; Ai, loss of apical adhesion only at the interface between clone cells and control cells; ApC, apical constriction; B, loss of basal adhesion; PS, pseudostratified.



**Supplementary Figure S4. Apical constriction does not lead to delamination but is sufficient to trigger basal displacement of cells in the pseudostratified epithelium.**

(A) Mean rate of basal positioning with standard error of the mean. To assess the effect of apical constriction, apical contractility of clone cells was increased 2.5 times (2.5X) and 5 times (5X) the control level in the flat epithelium and 3.5 times (3.5X) and 7 times (7X) the control level in the PS epithelium. ApC, apical constriction; CTL, control levels of apical contractility; PS, pseudostratified tissue.

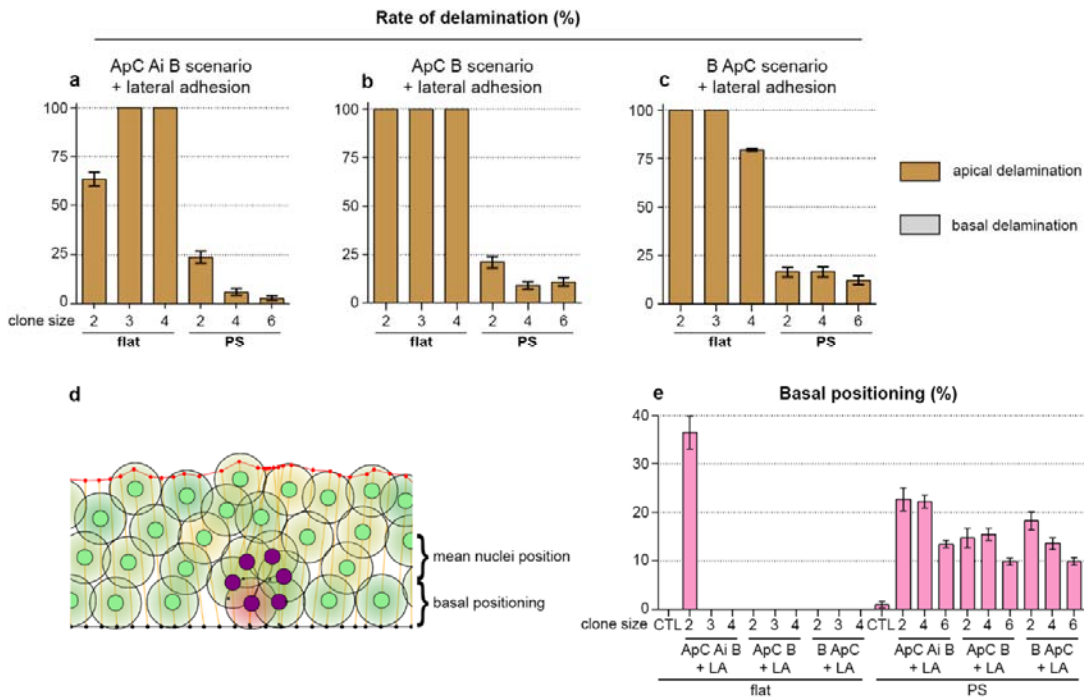


**Figure 7. A non-permissive basal compartment converts epithelial destabilization in the flat tissue into apical delamination.**

(A-C) Mean rates of delamination with standard error of the mean for all indicated scenarios tested in clones of various sizes in the presence of a non-permissive basal compartment. Each simulation was performed 200 times. (D) Example of a clone (magenta) that underwent the ApC B and lateral adhesion scenario, note that only some of the clone cells are considered basally positioned. (E) Rates of basal positioning for each tested scenario. A, loss of apical adhesion between clone cells and between clone cells and control cells; Ai, loss of apical adhesion only at the interface between clone cells and control cells; ApC, apical constriction; B, loss of basal adhesion; LA, lateral adhesion; PS, pseudostratified.

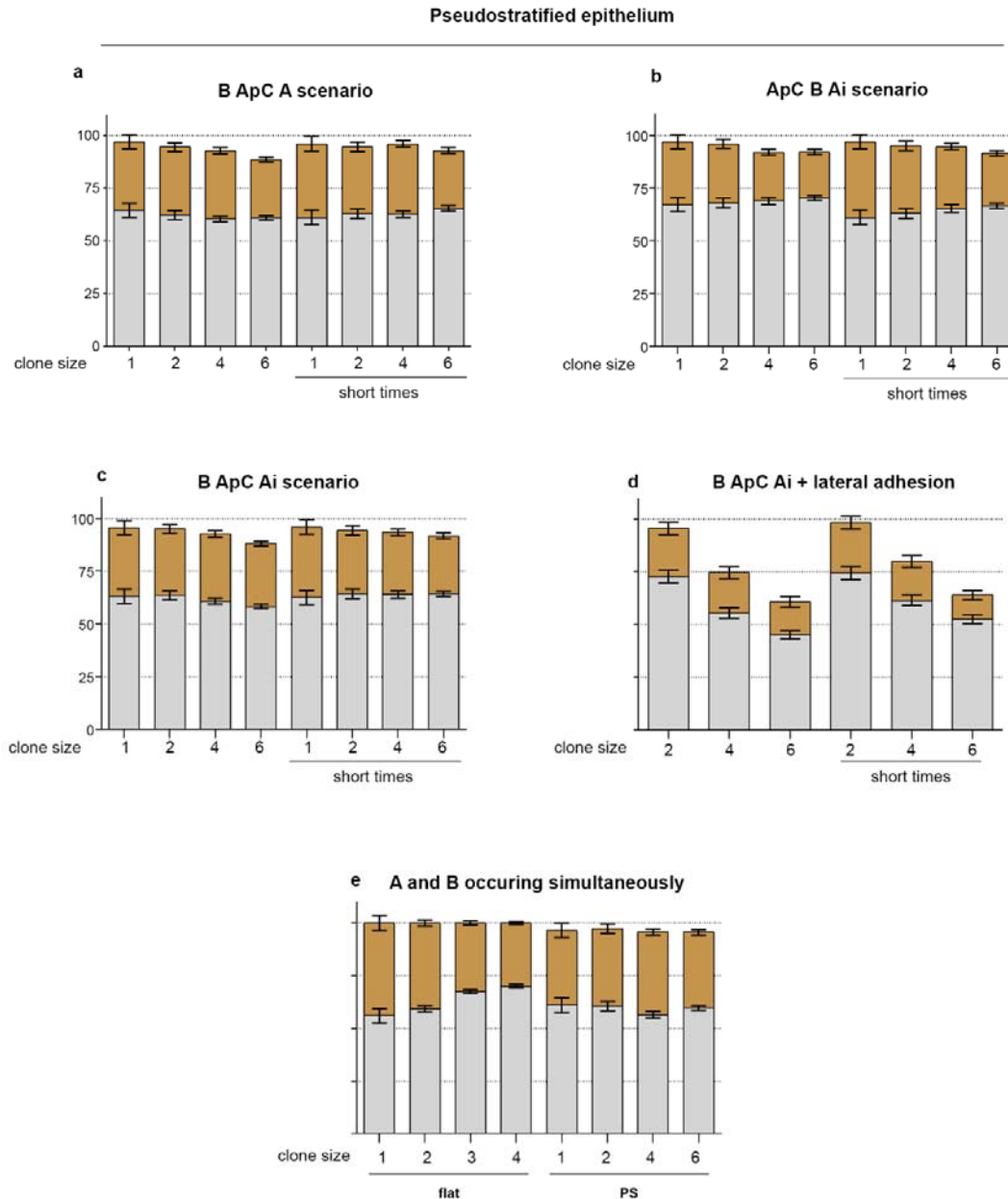


**Figure S5. Timing of epithelial destabilization has marginal influence on the directionality of delamination**

(A-D) Mean rates of delamination with standard error of the mean for all indicated scenarios tested in clones of various sizes in the pseudostratified epithelium. Scenarios have a time window of 20 hours to be implemented whereas under the “short times” condition all events must occur within 4 hours. (E) Mean rates of delamination with standard error of the mean

when events and A and B occur simultaneously. Each simulation was performed 200 times. A, loss of apical adhesion between clone cells and between clone cells and control cells; Ai, loss of apical adhesion only at the interface between clone cells and control cells; ApC, apical constriction; B, loss of basal adhesion; LA, lateral adhesion; PS, pseudostratified.

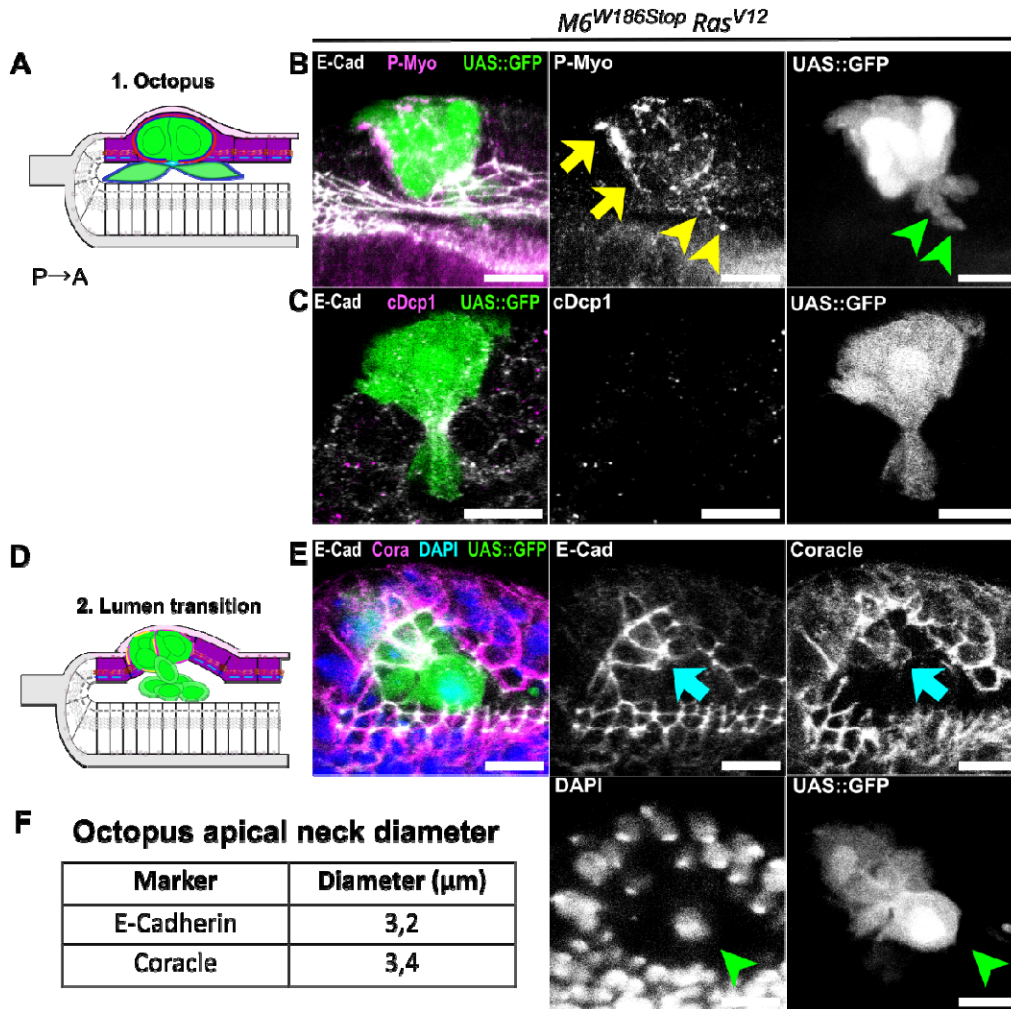


**Figure 8. Distribution of actomyosin force generator and preferential adhesion guide apical cell delamination**

(A, D) Schematic of an orthogonal section along the dorso-ventral axis of the *Drosophila* eye disc of the flat epithelium (purple). Mutant cells (green) apically constrict (A) into a dome-shaped octopus with apical protrusions and progressively translocate into the lumen (D).

(B, C, E) Heterozygous eye disc immunostained with anti-E-cad (grey) and anti-P-Myo (B, magenta) or anti-Drosophila caspase-1 (DCP-1) (C, magenta). Homozygous mutant cells for M6 (*M6<sup>W186Stop</sup>*) and oncogenic Ras cells express the clone marker UAS::GFP (green).

(B, C) During apical collective delamination, at the octopus stage, P-Myo appears enriched at the interface between mutant cells and their wild-type counterparts (yellow arrows) as well as at the tip of lumen protrusions (yellow arrowheads). No signs of caspase activation at this stage are detected, suggesting apical collective delamination occurs independently of apoptosis activation.

(E) During translocation of cells from the flat epithelium into the lumen a ring-like structure enriched in adhesion proteins (blue arrows) termed the “neck” it formed, with average diameter of  $3\mu\text{m}$  for cells to delaminate in the lumen (green arrowheads).

(F) Quantification of neck size performed on eye-antennal imaginal disc stained with anti-E-cadherin and anti-Coracle.

The scale bars represent 10  $\mu\text{m}$ . All images are single confocal optical sections with posterior to the left, anterior to the right.

### **Supplementary Movies legends**

#### **Supplementary Movie 1. Computational modelling of the eye-antennal imaginal disc using the EMT-simulator**

Initialization of each type of epithelium. All cells are control cells. Top panel: flat tissue, bottom panel: short pseudostratified (PS) tissue. Apical points are in red, basal points in black. Large nuclei correspond to mitosis. The flat epithelium reaches its stable configuration in about 5 hours. The pseudostratification with 2 to 3 pseudolayers takes about 20 hours to emerge and the stable configuration is reached at around 30 hours. In the PS tissue cells undergo interkinetic movement. For instance, the central cell labelled in magenta divides at 9, 23 and 34 during the simulation. Total duration 40 hours, time stamp in the top right corner.

#### **Supplementary Movie 2. The outcome of epithelial destabilization is sensitive to clone size in flat but not in pseudostratified epithelia**

Simulation of the ApC A B scenario in flat (top panel) and pseudostratified tissues (bottom panels) in a single cell (left panels) or a clone (right panels). ApC is implemented since the onset of simulation, A occurs at 40h, B occurs at 50h. Movie starts at 30h post initiation and stops at 80h of simulation.

#### **Supplementary Movie 3. Moderate cell adhesion does not prevent clone splitting in the pseudostratified epithelium but reverses directionality in the flat layer**

Simulation of the ApC Ai B scenario in flat (top panel) and pseudostratified tissues (bottom panels). ApC is implemented since the onset of simulation, Ai occurs at 40h, B occurs at 50h. Movie starts at 30h post initiation and stops at 80h of simulation.

#### **Supplementary Movie 4. Reinforced lateral adhesion between clones in pseudostratified epithelia suppresses clone splitting and favours basal delamination**

Simulation of the ApC Ai B and lateral adhesion between clone cells scenario in flat (top panel) and pseudostratified tissues (bottom panels). ApC is implemented since the onset of simulation, Ai occurs at 40h, B occurs at 50h. Movie starts at 30h post initiation and stops at 80h of simulation.

#### **Supplementary Movie 5. A non-permissive matrix prevents basal delamination in flat epithelia but does not abrogate the intrinsic basal directionality of delamination upon epithelial destabilization in the pseudostratified layer**

Simulation of the ApC Ai B and lateral adhesion between clone cells scenario in flat and pseudostratified tissues (top panels). Simulation of the ApC B and lateral adhesion between clone cells scenario in flat and pseudostratified tissues (middle panels). Simulation of the B ApC and lateral adhesion between clone cells scenario in flat and pseudostratified tissues (bottom panels). ApC is implemented since the onset of simulation for the ApC Ai B and ApC

B scenario and implemented at 50 hours for the B ApC scenario. Ai occurs at 40h, B occurs at 50h. Movie starts at 30h post initiation and stops at 80h of simulation.